Research Square

Preprints are preliminary reports that have not undergone peer review.
They should not be considered conclusive, used to inform clinical practice,
or referenced by the media as validated information.

IL-4 Licenses B Cell Activation Through Cholesterol Synthesis

Autumn York

agyork@uw.edu

University of Washington https://orcid.org/0000-0002-0331-043X

Holly Steach

Yale University

Jonathan Mattingly

University of Washington

Mathias Skadow

Yale University

Aimee Wu

University of Washington

Meijie Li

University of Washington

Fang Wang

Yale University

Shuting Chen

Yale University https://orcid.org/0000-0002-6892-5726

J. Brewer

Yale University

Walter Mowel

Yale University https://orcid.org/0000-0003-2393-4300

Will Bailis

University of Pennsylvania

Kevin Williams

UCLA https://orcid.org/0000-0001-8091-7924

Steven Bensinger

University of Southern California

Joseph Craft

Yale University https://orcid.org/0000-0002-1368-6756

Richard Flavell

Yale School of Medicine, Howard Hughes Medical Institute https://orcid.org/0000-0003-4461-0778

Letter

Keywords:

Posted Date: November 5th, 2026

DOI: https://doi.org/10.21203/rs.3.rs-11393609/v1

License: This work is licensed under a Creative Commons Attribution 4.0 International License.
Read Full License

Additional Declarations:
Yes there is potential Competing Interest. R.A.F. is a scientific advisor to GlaxoSmithKline. All other authors declare no competing interests.

The animal work in this manuscript is overseen by the University of Washington and Yale University Institutional Animal Care and Use Committees (IACUCs), which are overseen by the University of Washington Office of Animal Welfare (OAW) and the Yale Office of Animal Research Support (OARS), respectively.

IL-4 Licenses B Cell Activation Through Cholesterol Synthesis

Autumn G. York[1, 9 † *], Holly R. Steach[2,3 †], Jonathan R. Mattingly[1 †], Mathias H. Skadow[2], Aimee Wu[1], Meijie Aletta Li[1], Fang Wang[2], Shuting Chen[2], J. Richard Brewer[2], Walter K. Mowell[2], Will Bailis[6,7], Kevin J. Williams[5], Steven J. Bensinger[8], Joseph Craft[2,4*], Richard A. Flavell[2,9*]

[1]Department of Immunology, University of Washington, Seattle WA 98109, USA
[2]Department of Immunobiology, Yale University School of Medicine, New Haven, CT 06520, USA
[3]Program of Computational Biology and Bioinformatics, Yale University, New Haven, CT, USA
[4]Department of Internal Medicine (Rheumatology), Yale School of Medicine, New Haven, CT, USA
[5]Department of Medicine, David Geffen School of Medicine, University of California, Los Angeles, CA 90095, USA
[6]Division of Protective Immunity, Children's Hospital of Philadelphia, 19104, Philadelphia, PA, USA
[7]Department of Pathology and Laboratory Medicine, University of Pennsylvania, 19104, Philadelphia, PA, USA
[8]Department of Immunology and Immune Therapeutics, University of Southern California, 90033, Los Angeles, CA, USA
[9]Howard Hughes Medical Institute, Chevy Chase, MD, USA
[†]Authors contributed equally

*Corresponding authors: AGYork@uw.edu, joseph.craft@yale.edu, richard.flavell@yale.edu

Abstract

IL-4 is a pleiotropic cytokine that was first identified as a B cell co-mitogen over 30 years ago[1]. However, how IL-4 signaling mechanistically supports B cell proliferation is incompletely understood. Here, we find that the cholesterol biosynthetic program is transcriptionally upregulated by IL-4 signaling during the early B cell response to influenza virus infection and is required for B cell activation *in vivo*. Induction of lipid synthesis genes required both STAT6 and SREBP2 transcription factors, allowing IL-4 activated B cells to enter the cell cycle and proliferate in the absence of lipids. Genetic inhibition of *de novo* cholesterol synthesis via SREBP2 deletion reduced plasmablasts and subsequent germinal center B cell formation at steady state and following influenza infection. SREBP2-deficency blocked IL-4 mediated cell cycle entry, ER expansion, and subsequent proliferation in a cholesterol dependent manner. Further mechanistic studies revealed that ER cholesterol content promoted sustained STAT6 signaling associated with ER expansion and B cell survival. In sum, we demonstrate that the well-known ability of IL-4 to act as a B cell growth factor is through a previously unknown rewiring of specific lipid anabolic programs, relieving sensitivity of cells of environmental nutrient availability.

Introduction

Humoral immunity is critical for lasting protection following immunization or infection. In response to immunological challenge, antigen-specific B cells may differentiate into short-lived antibody-secreting cells (plasmablasts, PBs) or may alternatively be recruited into germinal centers where they undergo iterative rounds of diversification and selection to produce affinity matured cells that seed long-term protective populations including memory B cells and long-lived plasma cells. Generation of any of these effector subsets, however, is subject to a bottleneck imposed by initial B cell receptor (BCR) activation and expansion of naïve B cells. Early lymphocyte activation is driven by antigen receptor ligation, co-stimulation, and cytokines; yet even with the proper complement of signals, progression through cell division is constrained by multiple fitness checkpoints. Regulatory mechanisms that sense DNA damage or replication stress, nutrient availability (e.g. glucose, amino acids,), energetic status, redox balance, and protein homeostasis are conserved across eukaryotic cell types. As lymphocytes acquire specialized effector functions, they may encounter additional constraints imposed by the biochemical requirements of these state transitions, creating lineage- or context-dependent fitness checkpoints[2,3]. The cytokine interleukin (IL-)4 functions as a potent B cell co-mitogen[4], and while it is well known as a T follicular helper cell-derived mediator of germinal center positive selection[5], it has additionally been shown to be critical for initial expansion of B cells in various immune contexts[6,7]. How cytokine signals interface with these fitness checkpoints, whether by directly enforcing them or rewiring metabolism to satisfy their demands, remains an open area of investigation. Here, we investigate this relationship by dissecting the interplay between cytokine signaling and lipid metabolism during early B cell activation.

Cytokine signaling and other immune cell activation pathways have been shown to influence *de novo* lipid synthesis and export programs in T cells and macrophage[8-11]; however, the signals that regulate how B cells balance lipid homeostasis in response to different stimuli remains less clear. *De novo* lipid biosynthesis is regulated by the sterol-regulatory element binding protein (SREBP) family of transcription factors[12]. SREBP1, encoded by the gene *Srebf1*, and SREBP2, encoded by the gene *Srebf2,* regulate fatty acid and cholesterol biosynthesis programs, respectively[11,13,14]. SREBPs are held in the endoplasmic reticulum (ER) by chaperones SREBP cleavage-activating protein (SCAP) and Insig1/2 proteins, all of which are directly regulated by sterols present in the ER membrane. When sterol levels are low, Insigs dissociate from SCAP/SREBPs, permitting their translocation to the Golgi apparatus where SREBPs are cleaved by site 1 and 2 proteases (S1P and S2P, respectively; extended data Figure S1A). The active SREBP transcription factor domain translocates to the nucleus to mediate transcription of genes involved the fatty acid or cholesterol synthesis programs. The lipid biosynthesis programs are subject to feedback inhibition whereby synthesized lipids accumulate in the ER and associate with SCAP and Insig1/2 proteins to prevent activation of SREBPs. Additionally, the intermediate metabolite desmosterol ligates nuclear hormone Liver X Receptors (LXRs), which drive transcription of genes involved in efflux of both fatty acids and cholesterol, such as *Abca1*,

Abcg1, and *Apoe*[15]. Coordinate regulation of these positive and negative transcriptional programs together mediates metabolic homeostasis. It has been recently reported that SCAP-deficient B cells exhibit lower BCR, CD40, and Toll-like receptor 4 (TLR-4) responsiveness *in vitro,* as well as reduced numbers of germinal center B cells and antibody titers following vaccination[16]. These observations raise questions about the relative functional roles for SCAP targets SREBP1 and SREBP2. Inhibition of Stearoyl-CoA Desaturase-2 (SCD2), a SREBP1 target gene, has been shown to alter germinal center B cell responses[17]. Other studies found that IL-21/ROCK2 signaling promoted SREBP2 target gene expression in germinal center B cell and that ectopic expression of SREBP2 induced rapid plasma cell differentiation suggesting cholesterol or its intermediates support B cell differentiation and antibody production[18]. Prior to differentiation, it has been shown that LXRβ agonism impairs proliferation of activated T and B cells[8]. Collectively these data suggest a functional role for *de novo* lipid synthesis and efflux programs in GC B cell function; however, whether early pre-GC metabolic reprogramming is required for functional GC responses remains unknown.

Results

IL-4-dependent phase of early antiviral B cell activation engages lipid homeostasis pathways.

To better understand how early B cell activation impacts different arms of lipid homeostatic pathways, we isolated B cells from the mediastinal lymph node from Day 0 to Day 7 post PR8 influenza virus infection. We observed a marked upregulation in SREBP2 target genes (*Srebf2, Hmgcs1, Hmgcr, Sqle, Mvk, Dhcr24*) (Figure 1A, S1B) and SREBP1 target genes (*Fasn*, *Scd2*) (Figure 1B) that peaked around day 5 post infection. Notably, we observed a coordinate downregulation of LXR target genes (*Abca1, Abcg1*) at day 5 (Figure 1C), suggesting that early activation of B cells may promote lipid accumulation by engagement of *de novo* lipid synthesis programs, and inhibition of lipid efflux programs.

The early B cell response to influenza virus infection is dependent on IL-4 production by NK-T cells at interfollicular sites in the mediastinal lymph node[6]. NK-T cell IL-4 production peaks between days 3-5 post infection (tan boxes in Figure 1A-C, S1B), leading us to hypothesize that IL-4 receptor (IL-4R) signaling may be responsible for alterations in B cell lipid metabolic programs. To investigate the idea that IL-4 may be driving a lipid synthesis program in B cells, we performed single cell RNA sequencing (scRNAseq) on total CD19+ B cells sorted from mediastinal lymph nodes 4 days post-infection with PR8 influenza. Data were grouped into 5 major clusters using the Leiden algorithm and projected into UMAP space for visualization (Figure 1D, S1C)[19,20]. Cluster 4 expressed the highest amount of the IL-4-induced gene *Il4i1*, which we use as a proxy for IL-4 signaling, suggesting that these cells had recently been exposed to IL-4 (Figure 1D-E). In general, cells in cluster 4 exhibited lower expression of genes involved in cholesterol efflux and quiescence, and higher expression of genes involved in lipid synthesis and activation/differentiation (Figure 1D, 1E, S1C). To characterize and quantify functional relationships between IL-4R signaling (inferred from *Il4i1* expression)

and target gene expression, we used Conditional-Density Resampled Estimate of Mutual Information (DREMI), which quantifies statistical dependence between two variables while remaining agnostic to the form of the relationship and robust to the non-uniform distributions inherent in single-cell data[21]. When compared to the transcriptome-wide distribution of DREMI scores, several lipid metabolic genes (*Dhcr24*, *Sqle*, *Hmgcs1*, *Fasn*, *Acaca*) showed strong expression associations with *Il4i1* (Figure S1D). Visualizing these relationships revealed coordinated increases in activation-associated genes and lipid-anabolic genes alongside *Il4i1*, coupled with decreased expression of lipid-efflux and quiescence-associated genes (Figure S1E), suggesting that IL-4 signaling engaged a transcriptional program that promotes accumulation of actively synthesized lipids.

To confirm that IL-4R signaling was required for transcriptional changes in B cell lipid programs, we infected CD23 Cre+ control or CD23 Cre+/IL4R$^{Flox/Flox}$ (denoted IL4R cKO) mice with PR8 influenza. CD23 cre recombinase initiates Cre-mediated deletion in immature B cells and leads to efficient deletion in mature B cells of the spleen[22]. At day 5 post infection, we isolated B cells from the mediastinal lymph node and analyzed lipid gene expression by reverse transcription quantitative real-time polymerase chain reaction (qPCR). As expected, loss of B cell-specific IL-4R blunted induction of B cell activation genes *Prdm1* and *IL41i* (Figure S1F). Importantly, loss of B cell-specific IL-4R also blunted induction of both cholesterol and fatty acid synthesis genes (Figure 1F, S1G), without impacting lipid efflux gene expression (Figure 1G). In line with this data, transcription of lipid synthesis genes, along with canonical IL-4 target genes, were temporally induced by IL-4 treatment in *ex vivo* B cells, compared to those activated via BCR/CD40 alone (Figure 1H, S1H, S1I). Conversely, treatment with IL-21, a cytokine important for GC formation and *Sdc1* (CD138) induction (Figure S1J), did not impact the transcriptional regulation of lipid synthesis genes (Figure 1H, S1H), suggesting that increased *de novo* lipogenesis may be temporally restricted to pre-GC B cells via specific cytokine signals. Notably, BCR activation alone, or in combination with IL-4 or IL-21, strongly repressed transcription of LXR target genes (Figure S1K), suggesting that limiting lipid efflux is a conserved requirement for B cell activation *in vitro*. Finally, we hypothesized that the observed increase in lipid synthesis genes may require STAT6, a transcription factor that is downstream of IL-4 receptor activation, but not IL-21 receptor. Indeed, RNAseq analysis of *ex vivo* STAT6 knockout B cells indicated that STAT6 was required for IL-4 mediated regulation of SREBP1/2 target genes (Figure 1I). Combined, these data suggest that IL-4 signaling may support early B cell activation via induction of *de novo* lipid synthesis programs.

IL-4 circumvents a metabolic requirement for exogenous cholesterol

Sequential phases of B cell activation in secondary lymphoid tissues are spatially compartmentalized, creating dense areas of actively dividing cells[23] in which local nutrient availability may become limiting. Consistent with lipid availability imposing physiological constraints, previous studies have found that both cholesterol and fatty acid metabolism are required for proper GC formation[16,17,24], supporting the idea that B cell proliferation in

response to mitogenic stimuli such as antigen recognition requires lipids. Therefore, we hypothesized that in the absence of environmental lipids, signaling through IL-4R can compensate via upregulation of endogenous cholesterol synthesis to enable B cell activation. To test this, we developed an *in vitro* lipid free culture system where B cells were stimulated with B cell activating factor (BAFF), α-IgM and α-CD40 for 24-96 hours in a minimal media formulated to contain non-nutrient components of serum including insulin, transferrin, selenium, ethanolamine, and albumin but, importantly, no lipids. Relative to controls stimulated in 10% Fetal Bovine Serum (FBS), lipid deprivation caused reduced proliferation (Figure S2A). Notably, treatment with IL-4 promoted proliferation in both full serum and lipid depleted conditions compared to BCR activation alone (Figure S2A), suggesting that IL-4 signaling can circumvent the requirement for exogenous lipids.

We next asked whether exogenous lipid supplementation could mimic the effect of IL-4. B cells were activated in lipid free media supplemented with either Methyl-β-cyclodextrin (MBCD)-solubilized free cholesterol (herein denoted free cholesterol) or free fatty acids bound to endotoxin low bovine serum albumin (BSA). Of note, lipid solubilization by either method bypasses the requirement for vesicle-mediated uptake. Strikingly, free cholesterol addition enhanced B cell proliferation similarly to IL-4 (Figure 2A, 2B). Conversely, addition of neither oleic acid nor palmitic acid induced proliferation in lipid free media (Figure 2A, 2B), suggesting that cholesterol is uniquely required for B cell activation and proliferation. Similar enhancement of cellular proliferation with free cholesterol or IL-4, but not IL-21, were observed as early as 48h post BCR activation (Figure 2C). To determine how cholesterol and IL-4 regulate B cell proliferation, we assessed cell cycle status by co-staining with Ki-67 and 7AAD, allowing us to partition cells into G0, G1, S, and G2/M phases (representative gating in Figure 2D). Compared to full serum culture conditions, B cells cultured in lipid free media displayed a significant accumulation in G0, indicating that these cells were unable to enter cell cycle (Figure 2E). Notably, cell cycle progression was rescued by cholesterol in a dose dependent manner, or by addition of IL-4. Conversely, addition of IL-21 could not promote B cell proliferation or cell cycle entry in these culture conditions (Figure 2C, 2E), demonstrating a critical IL-4/cholesterol axis in licensing early activation of B cells.

We considered the possibility that free cholesterol may engage with IL-4R directly, allowing for spontaneous receptor activation even in the absence of cytokine ligation. To test this idea, we examined canonical IL-4 mediated gene expression after either IL-4 or free cholesterol addition in our *in vitro* lipid free system. Here, we found that IL-4 treatment strongly induced *Prdm1*, *IL4i1*, *Bcl6* and *Il4r* expression; however, free cholesterol treatment did not phenocopy this IL-4 induced transcriptional response (Figure 2F), indicating that while free cholesterol can mimic the ability of IL-4 to enable proliferation cell cycle entry, cholesterol alone cannot recapitulate all aspects of IL-4R signaling.

IL-4 drives flux into the mevalonate pathway

To verify that IL-4-mediated transcriptional induction of the cholesterol synthesis genes (Figure 1H, S1H) equated to altered flux into the mevalonate pathway, we employed gas chromatography-mass spectrometry (GC-MS) paired with ^{13}C-stable isotope enrichment studies to measure synthesized cholesterol in B cells (Figure S2B)[9,11]. In the presence of IL-4, we observed a significant increase in both the percentage of synthesized cholesterol and absolute amount of synthesized cholesterol in lipid free conditions (Figure 2G). IL-4 was also able to drive cholesterol synthesis in full serum conditions (Figure 2H), demonstrating that IL-4 is capable of modulating flux into the mevalonate pathway even in cholesterol replete conditions. Together, these data demonstrate that IL-4 signaling in B cells drives increased flux into the mevalonate pathway.

To determine if increased flux into the mevalonate pathway was required for IL-4 mediated proliferation, we utilized statins, a widely prescribed class of cholesterol-lowering drugs that target the rate-limiting enzyme of the mevalonate pathway, HMG-CoA reductase (HMGCR) (Figure S2B). Studies have reported mixed results on statins impacting humoral immunity following various types of vaccinations in humans; with the largest study suggesting that statin usage can reduce vaccine efficacy via unknown mechanisms[25-28]. To determine if statin-mediated reduction in *de novo* cholesterol synthesis can impact IL-4 mitogenic capacity, we activated *ex vivo* B cells with IL-4 in lipid-free conditions with and without Atorvastatin (Lipitor®; denoted ATV) the most abundantly prescribed statin. Importantly, Atorvastatin blocked the ability of IL-4 to induce proliferation and entry into the cell cycle in lipid free conditions (Figure 2I, 2J), suggesting that IL-4 signaling overcomes external lipid deprivation via upregulation of endogenous cholesterol synthesis. Addition of free cholesterol to ATV-treated B cells restored IL-4 mediated proliferation and cell cycle progression (Figure 2I, 2J). Together, these data show a critical role for cholesterol synthesis during IL-4 mediated B cell activation, suggesting a direct cellular mechanism through which statins may impact humoral immunity.

SREBP2 is required for IL-4 mediated proliferation and induction of cholesterol synthesis genes.

To confirm that IL-4 signaling was acting through SREBP2, we generated CD23 Cre+ Srebf2$^{flox/flox}$ conditional B cell knockout mice. In comparison to Cre-/Srebf2$^{Flox/Flox}$ controls, SREBP2 deficient B cells (denoted SREBP2 cKO) displayed a dramatic reduction in the expression of cholesterol synthesis genes in anti-IgM/CD40 conditions alone, and were unable to induce transcription of cholesterol synthesis genes in response to IL-4 treatment (Figure 3A). Further, SREBP2 cKO B cells exhibited impaired proliferation and entry into cell cycle downstream of BCR activation alone or in combination with IL-4 treatment (Figure 3B, 3C, S3A-B). In line with a failure to properly enter cell cycle, SREBP2 cKO B cells displayed accumulation of p21, which, in addition to its well-characterized roles in cellular stress responses, can restrict the transition from quiescence to proliferation through inhibition of cyclin-dependent kinase activity (Figure 3D)[29-31]. Importantly, treatment with free cholesterol rescued the pronounced proliferative and cell cycle defects associated with SREBP2 deficiency (Figure 3B-D, S3A-B). Addition of mevalonate, an intermediate metabolite in the

cholesterol synthesis pathway (Figure S2B), could not rescue proliferative defects in the SREBP2 cKO B cells (Figure S3C), further supporting the idea that free cholesterol in the key sterol metabolite required for cellular proliferation. Cholesterol is a key component of lipid rafts, the lipid-rich membrane microdomains that have been suggested to support both BCR and TCR signaling. Due to the importance of cholesterol in our system, we considered the possibility that SREBP2 cKO B cells may have impaired BCR engagement; however BCR-specific transcriptional programs were not impaired in SREBP2 deficient B cells 24h after BCR activation alone or with IL-4 treatment (Figure S3E). Together, these results suggest that defects in the SREBP2 cKO B cells arise after normal BCR initiation.

After 24h post activation, SREBP2 deficient B cells displayed a significant decrease in viability after BCR/CD40 engagement that was not rescued by IL-4 treatment (Figure 3E, S3D), suggesting that increased *de novo* synthesis of cholesterol may be required for the anti-apoptotic capacity of IL-4 when nutrients are limited. In support of this, addition of free cholesterol fully restored viability in SREBP2 cKO B cells activated with IL-4 in lipid-free conditions (Figure 3E, S3D). Prior studies have shown that BCR stimulation initiates extensive metabolic remodeling that, in the absence of appropriate secondary signals, can lead to cellular dysfunction and activation-induced apoptosis. We therefore asked whether the loss of viability in SREBP2-deficient B cells reflected increased apoptotic signaling[32]. Using western blot analysis, we found that SREBP2 cKO B cells displayed increased caspase-8 cleavage–the primary apical initiator of apoptosis–48h after IL-4 activation (Figure 3F). Importantly, the addition of free cholesterol reduced caspase-8 cleavage to levels observed in control cells (Figure 3F). Consistent with increased apoptosis, the pan-caspase inhibitor Z-VAD-FMK, denoted here as P-Caspi, rescued viability in SREBP2-deficient B cells in a dose-dependent manner after 48h stimulation with IL-4. (Figure 3G). These findings underscore the importance of *de novo* synthesized cholesterol following IL-4 signaling to prevent caspase-mediated cell death.

SREBP2 supports early plasmablast generation and subsequent GC formation

To explore the role of SREBP2 in B cells *in vivo*, we analyzed B-cell development in the bone marrow and spleen of control and SREBP2 cKO mice. The major B-cell subsets in both tissues, including early bone marrow stages and splenic transitional, follicular, and marginal zone populations, were comparable between the two groups by both frequency and number (Figure S4A-E), suggesting no developmental defects between genotypes. Additionally, we observed no difference in the total number of circulating B cells (Figure 4A, example gating in S4F, S5A-C). In contrast, we found a dramatic reduction in the number and frequency of circulating plasmablasts (Figure 4B), suggesting that, in specific B cell subsets, exogenous cholesterol from the environment (which is derived from lipoproteins), cannot compensate for loss of endogenously synthesized cholesterol. In line with our *in vitro* data, SREBP2 cKO plasmablasts displayed robust proliferation defects, as measured by Ki-67 staining (Figure 4C). Next, we examined the requirement for SREBP2 in GC B cell formation. To do so, we analyzed B cell populations in mesenteric lymph nodes, which are constantly

exposed to antigens derived from the diet and the microbiome, giving rise to ongoing germinal center reactions. In accordance with the circulation data, we observed no difference in the total number of B cells in the mesenteric lymph nodes between control and SREBP2 cKO animals (Figure 4D). However, SREBP2 cKO mice displayed significant reductions in number, frequency, and proliferative capacity of GC B cells (Figure 4E-G), similarly to reductions observed in SCAP-deficient mice[16]. Consistent with a reduction in GC B cells, we also observed a significant reduction in the number of total antibody secreting cells (ASCs) and a significant reduction in both the number and frequency of mature B220-, CD138+, IRF4+ plasma cells in the bone marrow (Figure 4H, 4I). Collectively, these data indicate that the SREBP2 transcriptional program supports plasmablast, plasma cell, and GC B cell formation *in vivo*.

To investigate whether SREBP2-deficiency impairs the humoral response to infection, we performed immune profiling on control and SREBP2 cKO mice infected intranasally with PR8 influenza. Again, we found no difference in the total number of B cells in circulation or in the lung-draining mediastinal lymph node 6 days post infection (Figure 4J). In line with steady-state data, we observed a significant reduction in the number of plasmablasts in circulation in the SREBP2 cKO mice 6 days post infection (Figure 4K), which corresponded with observed reductions in both number and frequency of plasmablasts within the mediastinal lymph node (Figure 4L). At day 10 post infection, frequencies of plasmablasts, GC B cells, and memory B cells were significantly reduced in the mediastinal lymph node of SREBP2 cKO mice (Figure 4M). These data suggest that SREBP2 is critical for supporting plasmablast responses and early germinal center formation in the context of influenza infection.

Flux through the mevalonate pathway is required for XBP1 splicing and ER expansion

Short-lived plasmablasts or long-lived plasma cells require expansion of the ER to support antibody production[33-35]. ER expansion in activated B cells is mediated by the transcription factor X-box binding protein 1 (XBP1)[36]. XBP1 functionality requires the removal of 26 nucleotides from the XBP1 mRNA, resulting in the spliced isoform[37], XBP1s, that is a key driver for plasmablast and plasma cell antibody secretion[33-35]. Markedly, SREBP2 cKO mice showed a significant reduction in circulating XBP1s+ plasmablasts at steady state (Figure 5A), further supporting a defect in plasmablast lineage commitment. In our lipid free culture system, we found that IL-4 significantly increased the spliced variant of XBP1 after BCR/CD40 activation (Figure 5B). In agreement with *in vivo* phenotypes (Figure 5A), SREBP2 cKO B cells failed to appropriately upregulate XBP1s (Figure 5B) *in vitro*. Importantly, free cholesterol rescued XBP1s transcript levels in SREBP2 cKO B cells (Figure 5B).

Cholesterol synthesis primarily occurs at the ER, where the amount of cholesterol is tightly regulated[12,38]. The ER is also the site where MβCD-solubilized (free) cholesterol initially accumulates[39], leading us to investigate how IL-4 and cholesterol impact ER expansion downstream of BCR/CD40 signaling. By staining with ER-

Tracker™ Green, a highly selective ER dye that binds sulphonylurea receptors of ATP-sensitive K+ channels prominent on ER, we found that IL-4 promotes the accumulation of ER mass in minimal media conditions (Figure 5C). Deletion of SREBP2 reduced ER mass after BCR/CD40 activation and blunted IL-4 mediated ER expansion (Figure 5C). Importantly, addition of free cholesterol restored ER mass in SREBP2 cKO B cells in a dose dependent manner (Figure 5D). Pharmacologic inhibition of *de novo* cholesterol synthesis with Atorvastatin also blocked IL-4 mediated ER expansion, which could also be rescued with free cholesterol (Figure S6A). Together, our data indicate that IL-4 induced XBP1 splicing and subsequent ER expansion is sensitive to *de novo* cholesterol synthesis.

Cholesterol synthesis promotes sustained STAT6 signaling in IL-4 activated B cells

After IL-4 receptor ligation, STAT6 is phosphorylated by JAK1/3, enabling phosphorylated STAT6 homodimers to enter the nucleus and activate transcription of IL-4 responsive genes, including XBP1[40-42]. In line with these previously published data, we also found a requirement for STAT6 in the induction of transcripts from the XBP1 promoter (Figure S6B). Because transcriptional induction of XBP1 provides the substrate for IRE1-mediated splicing and generation of transcriptionally active XBP1s, we next asked whether the cholesterol-dependent loss of XBP1s reflected a selective defect in the XBP1 program or broader disruption of STAT6-mediated gene expression. In line with this idea, loss of SREBP2 signaling completely blocked induction of STAT6-dependent gene expression (*Prdm1, IL4i1, IL4ra, Bcl6* and *Irf8*) downstream of IL-4R signaling (Figure 5E, S6C, S6D), indicating that cholesterol synthesis is required to maintain IL-4 mediated transcriptional programs. Since SREBP2-deficient B cells could not upregulate STAT6 target genes after IL-4 treatment (Figure 5E, S6D), we hypothesized that IL-4 mediated induction of cholesterol synthesis may be important for sustained STAT6 activation. Consistent with this idea, SREBP2 cKO B cells displayed undetectable levels of phospho-STAT6, without impacting total STAT6 levels, 48h after IL-4 activation (Figure 5F). Importantly, addition of free cholesterol fully restored STAT6 phosphorylation in SREBP2 deficient B cells (Figure 5F). Together, these data suggest that IL-4/STAT6-driven expression of cholesterol synthesis genes creates a feed forward cholesterol biosynthetic loop that promotes durable STAT6 activity. These findings suggest that IL-4-dependent cholesterol synthesis provides a metabolic secondary signal which licenses BCR-activated cells to overcome activation-induced cell cycle arrest and cell death.

Discussion

Lymphocyte activation involves a transition from quiescence and associated catabolic metabolism to a metabolic state with noted similarities to cancer cells such as heavy reliance on aerobic glycolysis for energy demands and increased nutrient requirements for biomass accumulation and cell division[2,43,44]. Specific nutrient requirements are met either by synthesis or by uptake from the extracellular environment. However, much like the intratumoral environment, dense proliferation of cells in lymphatic tissues may lead to local nutrient depletion and a metabolically challenging microenvironment. Following antigen receptor

ligation, lymphocytes require spatiotemporally distinct “second signals”. These include costimulatory receptor or cytokine signaling, which engage discrete programs that often involve remodeling of organelles and increased nutrient uptake or synthesis to meet changing biochemical demands[32,45,46]. Here, we find that the engagement of early antiviral B cell activation promotes *de novo* cholesterol synthesis in an IL-4/STAT6 dependent manner. IL-4/STAT6 mediated flux into the mevalonate pathway required SREBP2, the master transcriptional regulator of cholesterol synthesis. Loss of SREBP2 activity blocked IL-4 mediated entry into cell cycle, ER expansion, and proliferation *in vitro*. Importantly, loss of *de novo* synthesized cholesterol content did not fully ablate the B cell compartment in SREBP2 cKO mice. Instead, plasmablasts and GC B cells were significantly reduced in SREBP2 cKO mice, suggesting that the metabolic demands associated with B cell activation and differentiation cannot be met solely through exogenous cholesterol uptake.

BCR engagement itself places substantial metabolic demands on B cells, establishing a state in which lipid availability can become limiting and–in the absence of appropriate secondary signals–result in cell cycle arrest and activation-induced cell death[32]. Our findings suggest that cholesterol availability represents one metabolic constraint contributing to this gatekeeping function. BCR engagement has been reported to induce p53 and p21[29,47], with p53 exhibiting mevalonate pathway suppressive activity[48], suggesting a potential mechanism linking antigen receptor signaling, cholesterol availability, and the p21 accumulation observed here. Together, these observations raise the possibility that BCR engagement establishes a cholesterol-dependent threshold for cell cycle entry that can be overcome by an appropriate secondary signal. In line with this idea, we find that IL-4 promoted SREBP2-dependent cholesterol synthesis, which enabled BCR-activated cells to enter the cell cycle and avoid caspase-mediated cell death. Conversely, loss of SREBP2 rendered these cells refractory to the pro-proliferative and pro-survival effects of IL-4. Thus, IL-4-dependent cholesterol synthesis supplies BCR-activated cells a metabolic secondary signal to overcome activation-induced cell cycle arrest and cell death.

A hallmark of plasmablast cell lineage is the ability to produce high quantities of antibodies[49]. In addition to proliferative signals, this requires XBP1s-mediated expansion of the ER[35]. Our data suggest that IL-4 mediated ER expansion is sensitive to cholesterol content in the ER. We hypothesized that this process requires a threshold amount of cholesterol, and that IL-4 promotes endogenous cholesterol synthesis to relieve the reliance on exogenous cholesterol, which could be limiting in microenvironments in secondary lymphoid tissues containing dense foci of proliferative cells. Cholesterol is present at extremely low levels in the ER, rendering sensing mechanisms highly sensitive to small changes[39]. Our data are consistent with our previous work connecting SCAP-dependent cholesterol synthesis with ER biogenesis and activation of CD8+ T cells[9]. Considering the critical known role that ER to nuclear signaling plays in B cell activation and differentiation, it will be important for future studies to define how the molecular dynamics of inter-organellar crosstalk to license cell cycle entry, proliferation, and lineage commitment.

Mechanistic studies herein identified a requirement for SREBP2-induced cholesterol synthesis to maintain STAT6 activation. Loss of SREBP2 ablated STAT6 phosphorylation, reduced STAT6-mediated gene expression and the abundance of transcriptionally active XBP1s. This suggests a feed-forward cholesterol metabolic loop, where STAT6 activity upregulates flux into the mevalonate pathway to generate synthesized cholesterol at the ER, licensing ER expansion. In turn, ER cholesterol enhances the durability of STAT6 signaling to prevent apoptosis and enhance plasmablast lineage commitment (See schematic in Figure 5G). Since IL-4–dependent processes such as class-switch recombination, survival, and differentiation require prolonged transcriptional activity, rather than short signaling pulses, cholesterol-mediated maintenance of STAT6 activation ensures proper, durable humoral responses after antigen recognition[50,51]. As to how STAT6 engages SREBP2 at the molecular level to coordinately drive transcriptional changes of the cholesterol biosynthetic cassette remains unclear. SREBP processing and activation is highly sensitive to cholesterol levels in the ER. Thus, one possibility is that STAT6-mediated initial expansion of the ER reduces the percentage of cholesterol per unit of ER below the 5% threshold that promotes SREBP processing[38]. Alternatively, other unknown factors may engage with SREBP/SCAP to drive non-canonical SREBP processing events that are no longer dependent on ER cholesterol content. Future experiments beyond the scope of this study would be required to test these possibilities. Additionally, how ER cholesterol levels promote BCR activity and sustained STAT6 phosphorylation is also an important topic of future study. It is possible that ER cholesterol directly interacts with STAT6 or another unknown coregulator proteins. While our studies indicate that initial BCR and IL-4 signaling cascades are not impaired, it is possible that SREBP2-deficiency leads to lipid raft depletion after initial activation. Further investigation is needed to fully delineate how *de novo* cholesterol synthesis molecularly licenses early B cell activation, and future studies will be required to fully determine how ER cholesterol content influences the durability of STAT6 phosphorylation.

Finally, a 2018 study found that statins are used by more than 140 million people worldwide[52]. A number of studies have suggested that statin treatment, which blocks flux into the mevalonate pathway, impairs influenza vaccine efficacy in human patients over 65 years old, resulting in reduced effectiveness at preventing serious respiratory illness[23,25,26]. However other studies that focused on younger individuals and hepatitis A vaccines found no effect of statins on vaccine efficacy. Heterogeneity in human cohorts as well as confounding effects of age, vaccine type, and the effects of long-term statin treatment on other cell types obscure any conclusions that can be drawn from these previous studies about the direct effect of statins on B cell biology. Our work isolates a B cell intrinsic role for statin-mediated immune inhibition and defines a mechanism through which, at the cellular level, these drugs may impact vaccine strategies that largely depend upon humoral immunity. Similarly, previous studies report mixed results on statin-mediated alterations in the treatment of B cell lymphoma. Additional studies on the cell type specific roles of the mevalonate pathway in vaccine efficacy, cancer studies, and other disease models will be required to fully understand the impact of statin treatment on the immune system.

Acknowledgements:

We would like to thank J. Alderman, C. Lieber, L. Evangelisti, C. Hughes, and E. Hughes-Picard for technical and administrative assistance. AGY is supported by NIH 1DP2AG108923 and the Howard Hughes Medical Institute Hanna H. Gray Fellowship. HS was supported by the NSF GRFP. MHS was supported by the NSF GRFP and the Yale Trudeau Fellowship. WKM is supported by NIH T32-DK007356, and is the recipient of a Cancer Research Institute/Irvington Postdoctoral Fellowship. WB was supported by a K22 (NIAID 5K22AI141758). This work was supported by NIH grants R37AR40072 (JC and RAF) and R01AR074545 (JC); by the Colton Center for Autoimmunity at Yale (JC); by the Lupus Research Alliance (JC); and by the Howard Hughes Medical Institute (RAF and AGY).

Author contributions:

Conceptualization and design: HRS, AGY, JRM. Data acquisition and analysis- scRNAseq: HRS, AGY, JZ, RQ, MHS, YK Data acquisition and analysis- qPCR: AGY, JRM, HRS, AW, AL. Data acquisition and analysis- flow cytometry: HRS, JRM, AGY, MHS, SC, FW, AL, AW. Data acquisition and analysis- mass spectrometry: KJW, AGY, HRS, JRM. Technical support and suggestions: AW, AL, JZ, KJW, JRB, RQ, MHS, SC, WKM, JS, CH, WB, CC Writing- original draft: HRS Writing- review and edit: AGY, JRM, HRS, MHS, SJB, JC, RAF Project Administration: AGY, SJB, JC, RAF

Competing interests: R.A.F. is a scientific advisor to GlaxoSmithKline. All other authors declare no competing interests.

References:

1 Paul, W. E. History of interleukin-4. *Cytokine* **75**, 3-7 (2015). https://doi.org/10.1016/j.cyto.2015.01.038

2 Buck, M. D., Sowell, R. T., Kaech, S. M. & Pearce, E. L. Metabolic Instruction of Immunity. *Cell* **169**, 570-586 (2017). https://doi.org/10.1016/j.cell.2017.04.004

3 Domblides, C., Lartigue, L. & Faustin, B. Metabolic Stress in the Immune Function of T Cells, Macrophages and Dendritic Cells. *Cells* **7** (2018). https://doi.org/10.3390/cells7070068

4 Howard, M. *et al.* Identification of a T cell-derived b cell growth factor distinct from interleukin 2. *J Exp Med* **155**, 914-923 (1982). https://doi.org/10.1084/jem.155.3.914

5 Weinstein, J. S. *et al.* TFH cells progressively differentiate to regulate the germinal center response. *Nat Immunol* **17**, 1197-1205 (2016). https://doi.org/10.1038/ni.3554

6 Gaya, M. *et al.* Initiation of Antiviral B Cell Immunity Relies on Innate Signals from Spatially Positioned NKT Cells. *Cell* **172**, 517-533 e520 (2018). https://doi.org/10.1016/j.cell.2017.11.036

7 Mountz, J. D. *et al.* IL-4 receptor blockade is a global repressor of naive B cell development and responses in a dupilumab-treated patient. *Clin Immunol* **244**, 109130 (2022). https://doi.org/10.1016/j.clim.2022.109130

8 Bensinger, S. J. *et al.* LXR signaling couples sterol metabolism to proliferation in the acquired immune response. *Cell* **134**, 97-111 (2008). https://doi.org/10.1016/j.cell.2008.04.052

9 Kidani, Y. *et al.* Sterol regulatory element-binding proteins are essential for the metabolic programming of effector T cells and adaptive immunity. *Nat Immunol* **14**, 489-499 (2013). https://doi.org/10.1038/ni.2570

10 Hsieh, W. Y. *et al.* Toll-Like Receptors Induce Signal-Specific Reprogramming of the Macrophage Lipidome. *Cell Metab* **32**, 128-143.e125 (2020). https://doi.org/10.1016/j.cmet.2020.05.003

11 York, A. G. *et al.* Limiting Cholesterol Biosynthetic Flux Spontaneously Engages Type I IFN Signaling. *Cell* **163**, 1716-1729 (2015). https://doi.org/10.1016/j.cell.2015.11.045

12 Horton, J. D., Goldstein, J. L. & Brown, M. S. SREBPs: activators of the complete program of cholesterol and fatty acid synthesis in the liver. *J Clin Invest* **109**, 1125-1131 (2002). https://doi.org/10.1172/JCI15593

13 Kennewick, K. T. & Bensinger, S. J. Decoding the crosstalk between mevalonate metabolism and T cell function. *Immunol Rev* **317**, 71-94 (2023). https://doi.org/10.1111/imr.13200

14 Mattingly, J. R., Wu, A. & York, A. G. Regulation of Adaptive Immunity by Lipid Post-translational Modifications. *Immune Netw* **25**, e11 (2025). https://doi.org/10.4110/in.2025.25.e11

15 Spann, N. J. *et al.* Regulated accumulation of desmosterol integrates macrophage lipid metabolism and inflammatory responses. *Cell* **151**, 138-152 (2012). https://doi.org/10.1016/j.cell.2012.06.054

16 Luo, W. *et al.* SREBP signaling is essential for effective B cell responses. *Nat Immunol* **24**, 337-348 (2023). https://doi.org/10.1038/s41590-022-01376-y

17 Zhou, X. *et al.* Stearoyl-CoA Desaturase-Mediated Monounsaturated Fatty Acid Availability Supports Humoral Immunity. *Cell Rep* **34**, 108601 (2021). https://doi.org/10.1016/j.celrep.2020.108601

18 Trapnell, C. *et al.* Differential gene and transcript expression analysis of RNA-seq experiments with TopHat and Cufflinks. *Nat Protoc* **7**, 562-578 (2012). https://doi.org/10.1038/nprot.2012.016

19 Traag, V. A., Waltman, L. & van Eck, N. J. From Louvain to Leiden: guaranteeing well-connected communities. *Sci Rep* **9**, 5233 (2019). https://doi.org/10.1038/s41598-019-41695-z
20 Leland McInnes, J. H., James Melville. UMAP: Uniform Manifold Approximation and Projection for Dimension Reduction. *ArXiv e-prints* (2018). https://doi.org/https://doi.org/10.48550/arXiv.1802.03426
21 Krishnaswamy, S. *et al.* Systems biology. Conditional density-based analysis of T cell signaling in single-cell data. *Science* **346**, 1250689 (2014). https://doi.org/10.1126/science.1250689
22 Kwon, K. *et al.* Instructive role of the transcription factor E2A in early B lymphopoiesis and germinal center B cell development. *Immunity* **28**, 751-762 (2008). https://doi.org/10.1016/j.immuni.2008.04.014
23 Omer, S. B. *et al.* Impact of Statins on Influenza Vaccine Effectiveness Against Medically Attended Acute Respiratory Illness. *J Infect Dis* **213**, 1216-1223 (2016). https://doi.org/10.1093/infdis/jiv457
24 Trindade, B. C. *et al.* The cholesterol metabolite 25-hydroxycholesterol restrains the transcriptional regulator SREBP2 and limits intestinal IgA plasma cell differentiation. *Immunity* **54**, 2273-2287 e2276 (2021). https://doi.org/10.1016/j.immuni.2021.09.004
25 Black, S., Nicolay, U., Del Giudice, G. & Rappuoli, R. Influence of Statins on Influenza Vaccine Response in Elderly Individuals. *J Infect Dis* **213**, 1224-1228 (2016). https://doi.org/10.1093/infdis/jiv456
26 Mehrbod, P., Omar, A. R., Hair-Bejo, M., Haghani, A. & Ideris, A. Mechanisms of action and efficacy of statins against influenza. *Biomed Res Int* **2014**, 872370 (2014). https://doi.org/10.1155/2014/872370
27 Davaro, F. *et al.* 3-Hydroxyl-3-methylglutaryl coenzyme A (HMG-CoA) reductase inhibitor (statin)-induced 28-kDa interleukin-1beta interferes with mature IL-1beta signaling. *J Biol Chem* **289**, 16214-16222 (2014). https://doi.org/10.1074/jbc.M114.571505
28 Pereira, J. P., Kelly, L. M. & Cyster, J. G. Finding the right niche: B-cell migration in the early phases of T-dependent antibody responses. *Int Immunol* **22**, 413-419 (2010). https://doi.org/10.1093/intimm/dxq047
29 Spencer, S. L. *et al.* The proliferation-quiescence decision is controlled by a bifurcation in CDK2 activity at mitotic exit. *Cell* **155**, 369-383 (2013). https://doi.org/10.1016/j.cell.2013.08.062
30 Abbas, T. & Dutta, A. p21 in cancer: intricate networks and multiple activities. *Nat Rev Cancer* **9**, 400-414 (2009). https://doi.org/10.1038/nrc2657
31 Koberlin, M. S. *et al.* A fast-acting lipid checkpoint in G1 prevents mitotic defects. *Nat Commun* **15**, 2441 (2024). https://doi.org/10.1038/s41467-024-46696-9
32 Akkaya, M. *et al.* Second signals rescue B cells from activation-induced mitochondrial dysfunction and death. *Nat Immunol* **19**, 871-884 (2018). https://doi.org/10.1038/s41590-018-0156-5
33 Taubenheim, N. *et al.* High rate of antibody secretion is not integral to plasma cell differentiation as revealed by XBP-1 deficiency. *J Immunol* **189**, 3328-3338 (2012). https://doi.org/10.4049/jimmunol.1201042
34 Hu, C. C., Dougan, S. K., McGehee, A. M., Love, J. C. & Ploegh, H. L. XBP-1 regulates signal transduction, transcription factors and bone marrow colonization in B cells. *EMBO J* **28**, 1624-1636 (2009). https://doi.org/10.1038/emboj.2009.117
35 Todd, D. J. *et al.* XBP1 governs late events in plasma cell differentiation and is not required for antigen-specific memory B cell development. *J Exp Med* **206**, 2151-2159 (2009). https://doi.org/10.1084/jem.20090738

36 Shaffer, A. L. *et al.* XBP1, downstream of Blimp-1, expands the secretory apparatus and other organelles, and increases protein synthesis in plasma cell differentiation. *Immunity* **21**, 81-93 (2004). https://doi.org/10.1016/j.immuni.2004.06.010
37 Yoshida, H., Matsui, T., Yamamoto, A., Okada, T. & Mori, K. XBP1 mRNA is induced by ATF6 and spliced by IRE1 in response to ER stress to produce a highly active transcription factor. *Cell* **107**, 881-891 (2001). https://doi.org/10.1016/s0092-8674(01)00611-0
38 Radhakrishnan, A., Goldstein, J. L., McDonald, J. G. & Brown, M. S. Switch-like control of SREBP-2 transport triggered by small changes in ER cholesterol: a delicate balance. *Cell Metab* **8**, 512-521 (2008). https://doi.org/10.1016/j.cmet.2008.10.008
39 Sandhu, J. *et al.* Aster Proteins Facilitate Nonvesicular Plasma Membrane to ER Cholesterol Transport in Mammalian Cells. *Cell* **175**, 514-529 e520 (2018). https://doi.org/10.1016/j.cell.2018.08.033
40 Iwakoshi, N. N. *et al.* Plasma cell differentiation and the unfolded protein response intersect at the transcription factor XBP-1. *Nat Immunol* **4**, 321-329 (2003). https://doi.org/10.1038/ni907
41 Hou, J. *et al.* An interleukin-4-induced transcription factor: IL-4 Stat. *Science* **265**, 1701-1706 (1994). https://doi.org/10.1126/science.8085155
42 Takeda, K. *et al.* Essential role of Stat6 in IL-4 signalling. *Nature* **380**, 627-630 (1996). https://doi.org/10.1038/380627a0
43 Boothby, M. & Rickert, R. C. Metabolic Regulation of the Immune Humoral Response. *Immunity* **46**, 743-755 (2017). https://doi.org/10.1016/j.immuni.2017.04.009
44 Jellusova, J. & Rickert, R. C. A Brake for B Cell Proliferation: Appropriate responses to metabolic stress are crucial to maintain B cell viability and prevent malignant outgrowth. *Bioessays* **39** (2017). https://doi.org/10.1002/bies.201700079
45 Klein Geltink, R. I. *et al.* Mitochondrial Priming by CD28. *Cell* **171**, 385-397 e311 (2017). https://doi.org/10.1016/j.cell.2017.08.018
46 Saravia, J., Raynor, J. L., Chapman, N. M., Lim, S. A. & Chi, H. Signaling networks in immunometabolism. *Cell Res* **30**, 328-342 (2020). https://doi.org/10.1038/s41422-020-0301-1
47 Lee, H. *et al.* A p53 axis regulates B cell receptor-triggered, innate immune system-driven B cell clonal expansion. *J Immunol* **188**, 6093-6108 (2012). https://doi.org/10.4049/jimmunol.1103037
48 Moon, S. H. *et al.* p53 Represses the Mevalonate Pathway to Mediate Tumor Suppression. *Cell* **176**, 564-580 e519 (2019). https://doi.org/10.1016/j.cell.2018.11.011
49 Nutt, S. L., Hodgkin, P. D., Tarlinton, D. M. & Corcoran, L. M. The generation of antibody-secreting plasma cells. *Nat Rev Immunol* **15**, 160-171 (2015). https://doi.org/10.1038/nri3795
50 Chevrier, S., Kratina, T., Emslie, D., Tarlinton, D. M. & Corcoran, L. M. IL4 and IL21 cooperate to induce the high Bcl6 protein level required for germinal center formation. *Immunol Cell Biol* **95**, 925-932 (2017). https://doi.org/10.1038/icb.2017.71
51 Wang, W., Wang, L. & Zha, B. The roles of STAT6 in regulating B cell fate, activation, and function. *Immunol Lett* **233**, 87-91 (2021). https://doi.org/10.1016/j.imlet.2021.02.006
52 Blais, J. E. *et al.* Trends in lipid-modifying agent use in 83 countries. *Atherosclerosis* **328**, 44-51 (2021). https://doi.org/10.1016/j.atherosclerosis.2021.05.016

Methods

Mice

Mice were housed at a temperature of 72 °F (22 °C) and humidity of 30–70% in a 12-h light/dark cycle with ad libitum access to food and water. Female mice aged 8–10 weeks at the start of the experiment were used throughout. Mice were bred and housed in the facilities of the Yale Animal Resources Center and University of Washington vivarium. C57BL/6N animals were purchased originally from Charles River and maintained in a breeding colony. C57BL/6J, B6.129S2(C)-Stat6tm1Gru/J (Stat6 Knockout), CD23 Cre (Jax) and Srebf2tm1Jdh/J (Srebp2 flox) were purchased from Jackson Laboratories.

Infections

Mice were anesthetized i.p. with Ketamine/Xylazine (100 mg/kg body) and intranasally infected with 200 PFU of Influenza virus A/Puerto Rico/8/1934 (PR8) H1N1 strain expressing the LCMV gp33-41 epitope (PR8-33).[1] Influenza virus was kindly provided by Drs. Susan Kaech and Jun Siong Low.

B Cell Isolation and Transfers

Single-cell suspensions were prepared from the spleens and lymph nodes of donor mice. Mature B2 B cells were enriched using immunomagnetic negative selection (StemCell Technologies, 19854). For proliferation analysis, isolated B cells were labeled at a concentration of 20 x 10^6 cells/mL in 1XPBS containing 5 uM CellTrace™ Violet (Invitrogen, C34557) for 12 minutes at 37˚C. The labeling reaction was quenched by washing with RPMI supplemented with 10% FBS, 2 mM L-glutamine, 50 U/ml Pen Strep, and 55 µM 2-Me prior to downstream culture.

Cell Culture

Isolated B cells were activated at a concentration of 2E6 cells/mL with 10 ng/mL recombinant mouse BAFF (R&D systems, 8876-BF-010) 5 µg/mL goat anti-mouse IgM (Jackson Immunoresearch, 115-006-075), 1 µg/mL anti-CD40 (BioXcell, BP0016-2), recombinant mouse IL-4 (Peprotech, 214-14) or recombinant mouse IL-21 (Biolegend, 574504).

Cell culture media contained RPMI (Gibco, 21870076) supplemented with 10% FBS (Cytiva, SH30396.03) or a 1:100 dilution of a cocktail containing Insulin, Transferrin, Selenium, Ethanolamine (Gibco, 51500056), and 5mg/mL endotoxin-low recombinant human albumin (Sigma, A9731). All cell culture media contained 2 mM L-glutamine, 50 U/ml Pen Strep and 55 µM 2-Me.

BSA-conjugated 16:0 palmitate and 18:1 oleic acid were generated as previously described and added at a concentration of 25 µM. MbCD-cholesterol (Sigma, C4951) was added at a concentration of 8ug/mL

cholesterol unless otherwise specified. Atorvastatin (Sigma, PHR1422) was solubilized in DMSO and added at indicated concentrations.

Flow Cytometry

Single cell suspensions harvested from cell culture or isolated from spleen, mediastinal lymph nodes, or bone marrow were incubated with Fc-block for 10min followed by viability stain and select surface antibodies for 15min. eBioscience Foxp3 / Transcription Factor Staining Buffer Set (Thermo, 00-5523-00) was used for intracellular transcription factor staining according to manufacturer instructions. For metabolic FACS analysis, cells were incubated at a final concentration 100nM ER-Tracker Green™ (Invitrogen, E34251) in HBSS +Ca/Mg for 15 minutes at 37˚C according to manufacturer instructions. All antibodies and key reagents used for flow cytometry in this study are listed in the table below. (Need Abs from Yale)

Reagent	Vendor	Identifier
Blimp-1 PE (E57)	Biolegend	Cat# 150005
B220/CD45R APC-Cy7 (RA3-6B2)	Biolegend	Cat# 103223
B220/CD45R FITC (RA3-6B2)	Biolegend	Cat# 103205
CD3 BV510 (17A2)	Biolegend	Cat# 100234
CD38 PE-Cy7 (90)	Biolegend	Cat# 102717
CD138 APC (281-2)	Biolegend	Cat# 142505
CD138 BV711 (281-2)	Biolegend	Cat# 142519
eBioscience Fixable Viability Dye eFlour 780	Invitrogen	Cat# 65-0866-14
eBioscience Fixable Viability Dye eFlour 780	Invitrogen	Cat# 65-0865-14
Fc-Block	Cytek	Cat# 70-0161-U500
F4/80 BV510 (BM8)	Biolegend	Cat# 123135
GL-7 eFlour 450 (GL-7)	Invitrogen	Cat# 48-5902-82
Goat anti-mouse IgG (H+L) AF350	Invitrogen	Cat# A-11045
IgD BV605 (11-26c.2a)	Biolegend	Cat# 405727
IRF4 PE (IRF4.3E4)	Biolegend	Cat# 646403
IRF4 PE-Cy7 (TRF4.3E4)	Biolegend	Cat# 646413
Ki-67 BUV395 (B56)	BD	Cat# 564071
TER-119 BV510 (TER-119)	Biolegend	Cat# 116237
XBP1s BV421 (Q3-695)	BD	Cat# 563382
7-AAD	Molecular Probes	Cat# A1310

Multi-color cytometry was performed on the LSR II flow cytometer (BD biosciences), CytoFLEX S (Beckman Coulter), or LSRFortessa flow cytometer (BD Biosciences) and analyzed with FlowJo v10.6.2 or FlowJo v10.10.0.

Western Blot

Purified B cells were cultured for 24-48h hours in specified conditions. Cells were lysed directly in RIPA buffer supplemented with Halt protease and phosphatase inhibitor cocktail before 1:1 dilution with 2x Laemmli loading buffer and then boiled at 95°C for 10min. Protein extracts were separated on gradient 4% to 12% NuPAGE Bis–Tris Mini protein gels (Invitrogen) and then transferred to a nitrocellulose membrane (Invitrogen). After blocking for 1 hour in PBS containing 0.1% Tween 20 (PBS-T) and 5% nonfat milk or 5% BSA, the membrane was probed with anti-p21 Waf1/Cip1 (Cell Signaling, 37543, clone E2R7A), anti-Cleaved Caspase-8 (Asp387) (Cell Signaling, 8592, clone D5B2) anti-phospho-STAT6 (Tyr641) (Cell Signaling, 9361), anti-STAT6 (Cell Signaling, 5397, clone D3H4), anti-β-actin (Cell Signaling, 4967) diluted into PBS-T with 5% nonfat milk or 5% BSA overnight. Membranes were washed 3x with PBS-T, followed by a 30-minute room temperature incubation with mouse (Cell Signaling, 7076) or rabbit (Cell Signaling, 7074) secondary antibodies conjugated to horseradish peroxidase diluted in 5% nonfat milk or 5% BSA in PBS-T. Membranes were washed as before and then developed using Pierce Supersignal West Pico/Femto/Atto detection kits and imaged with an Invitrogen iBright 1500 imaging system.

Quantitative PCR

Purified B cells were cultured for 24-48 hours in specified conditions. Dead or dying cells were depleted using immunomagnetic negative selection (STEMCELL technologies). RNA was isolated using a phenol-chloroform extraction and cDNA was generated using Bio-Rad iScript cDNA synthesis kit or Applied Biosystems high-capacity cDNA reverse transcription kit. Pre-validated primers were all ordered through Sigma. Bio-Rad iTag Universal Sybr Green Supermix and Bio-Rad CFX6 real-time PCR detection system or Thermo PowerTrack SYBR Green Master Mix and Quantstudio 5 real-time PCR detection system were used for quantitative analysis. Fold change related to the control group was calculated using $2^{-\Delta\Delta CT}$ method with Actb as the reference gene.

Bulk RNA Sequencing

For bulk RNA sequencing, purified B cells were cultured for 72 hours in specified conditions. Dead or dying cells were depleted using immunomagnetic negative selection (STEMCELL technologies) and RNA was extracted using Trizol and Qiagen RNeasy Kit. Technical duplicates were submitted to the Yale Center for Genome Analysis for cDNA synthesis and RNA sequencing. Libraries with unique barcodes were pooled and sequenced on Illumina NovaSeq S1 to produce 100 bp paired-end reads following manufacturer's protocol. Raw reads from RNA-sequencing were aligned to the mouse genome mm10 using Kallisto[2]. Subsequently, differential expression analysis between groups was performed with DESeq2[3].

Single-Cell RNA Sequencing

For scRNAseq, single cell suspensions from mesenteric lymph nodes of 3 pooled mice on day 4 of PR8-gp33 Influenza infection were sorted on a Sony SH800 cell sorter. Populations of CD3+, CD19+, and CD3-CD19-CD45+ were pooled in a 1:1:1 ratio. Cells from pooled and approximately 10,000 cells were loaded onto a Chromium Controller (10x Genomics). Single-cell RNA-seq libraries were prepared using the Chromium Single Cell 5′ v2 Reagent Kit (10x Genomics) according to manufacturer's protocol and libraries were sequenced on the Illumina NovaSeq.

For data preprocessing, mRNA library reads were aligned to the mouse genome mm10 and quantified using CellRanger count[4]. Data was subsequently analyzed using Seurat (version 4.0)[5–8]. Data was first filtered to exclude cells in the 5th and 95th percentiles of library size and number of expressed genes, as well as cells with more than 5% mitochondrial transcripts, and include only genes expressed in more than 3 cells. Data was then normalized in terms of log (CPM/100 + 1), where CPM stands for counts per million (meaning that the sum of all gene-levels is equal 1,000,000). After normalization, we used ALRA (Adaptively-Thresholded Low Rank Approximation)[9] to impute the matrix and fill in the technical dropout values. Subsequently, principal component analysis (PCA) was used to reduce data dimensionality followed by t-Distributed Stochastic Neighbor Embedding (t-SNE),[10] a non-linear dimensionality reduction method. Louvain graph-based clustering[7] was then used to generate clusters that were overlaid on the t-SNE coordinates to discern cell subpopulations.

Two individual clusters comprised B cells and were extracted into a new data subset. Monocle 2 was then used to perform semi-supervised ordering to specifically learn a trajectory defined by cellular activation. In a separate analysis, cells were subsetted based on imputed expression of CD19 which yielded similar results when subject to the same downstream trajectory analysis (*data not shown*). Btg2 and Myc were selected as "bellwether" genes to identify naïve and activated cells, respectively. The top 1000 genes that co-varied in either direction were determined and used to order cells along a developmental trajectory between these two states and assign a pseudotime value to each cell using reverse graph embedding.

U^{13}C-glucose labeling of cells and Isotope Enrichment Analysis

B cells activated under specified conditions were labeled in media containing 50% U^{13}C-glucose. Cells were harvested at 72 hours and Annexin V+ dead/dying cells were depleted using immunomagnetic negative selection (STEMCELL technologies). Isotopomeric Spectral Analysis (ISA) was performed as previously described[11].

Shotgun Lipidomic Analysis

B cells were activated under specified conditions. Cells were harvested at 72 hours and Annexin V+ dead/dying cells were depleted using immunomagnetic negative selection (STEMCELL technologies).

Technical quadruplicates were analyzed on the Sciex Lipidyzer Platform and data analysis performed on Lipidyzer software as previously described[12]. Quantitative values were normalized to cell counts and lipid species with more than two missing values due to technical dropout were excluded from analysis.

Statistical Analysis

Experiments were conducted with technical and biological replicates at an appropriate sample size as estimated by our prior experience. No statistical methods were used to predetermine sample size. No methods of randomization and no blinding were applied. All data were replicated independently at least once as indicated in the figure legends, and all attempts to reproduce experimental data were successful. For all bar graphs, mean and S.D. are shown. All statistical analysis was performed using GraphPad Prism 7 or newer. p-values <0.05 were considered significant (*p<0.05, **p<0.01; ***p<0.005, **** p<0.0001); p-values >0.05; non-significant (ns). All sample sizes and statistical tests used are detailed in figure legends.

Methods References

1. Gaya, M. *et al.* Initiation of Antiviral B Cell Immunity Relies on Innate Signals from Spatially Positioned NKT Cells. *Cell* **172**, 517-533.e20 (2018).
2. Bray, N. L., Pimentel, H., Melsted, P. & Pachter, L. Near-optimal probabilistic RNA-seq quantification. *Nat. Biotechnol.* **34**, 525–527 (2016).
3. Love, M. I., Huber, W. & Anders, S. Moderated estimation of fold change and dispersion for RNA-seq data with DESeq2. *Genome Biol.* **15**, (2014).
4. Zheng, G. X. Y. *et al.* Massively parallel digital transcriptional profiling of single cells. *Nat. Commun.* **8**, 1–12 (2017).
5. Hao, Y. *et al.* Integrated analysis of multimodal single-cell data. *bioRxiv* 2020.10.12.335331 (2020). doi:10.1101/2020.10.12.335331
6. Stuart, T. *et al.* Comprehensive Integration of Single-Cell Data. *Cell* **177**, 1888-1902.e21 (2019).
7. Butler, A., Hoffman, P., Smibert, P., Papalexi, E. & Satija, R. Integrating single-cell transcriptomic data across different conditions, technologies, and species. *Nat. Biotechnol.* **36**, 411–420 (2018).
8. Satija, R., Farrell, J. A., Gennert, D., Schier, A. F. & Regev, A. Spatial reconstruction of single-cell gene expression data. *Nat. Biotechnol.* **33**, 495–502 (2015).
9. Linderman, G. C., Zhao, J. & Kluger, Y. Zero-preserving imputation of scRNA-seq data using low-rank approximation. *bioRxiv* 397588 (2018). doi:10.1101/397588
10. Van Der Maaten, L. & Hinton, G. *Visualizing Data using t-SNE*. *Journal of Machine Learning Research* **9**, (2008).
11. Williams, K. J. *et al.* An essential requirement for the SCAP/SREBP signaling axis to protect cancer cells from lipotoxicity. *Cancer Res.* **73**, 2850–2862 (2013).
12. Hsieh, W. Y. *et al.* Toll-Like Receptors Induce Signal-Specific Reprogramming of the Macrophage Lipidome. *Cell Metab.* **32**, 128-143.e5 (2020).

Figure 1: IL-4 drives cholesterol synthesis gene expression *in vivo*.

a. Quantitative PCR (qPCR) analysis of cholesterol synthesis genes in B cells isolated from the mediastinal lymph node after infection with 200 PFU of Influenza virus A/Puerto Rico/8/1934 (PR8) H1N1 strain expressing the LCMV gp33-41 epitope (PR8-33) at listed time points. Shaded section indicates the peak of IL-4 production by NK-T cells.
b. qPCR analysis of fatty acid synthesis genes in B cells isolated from the mediastinal lymph as in (A)
c. qPCR analysis of lipid efflux genes in B cells isolated from the mediastinal lymph node as in (A)
d. UMAP visualization of murine B cells 4 days post infection (dpi) with PR8 influenza A virus as in (A) colored by Leiden clusters (top left) or relative gene expression values
e. Heatmap displaying gene expression from scRNAseq cluster analysis of murine B cells 4dpi with PR8 influenza A virus as in (A). Colors indicate z-scored expression values across all clusters.
f. qPCR analysis of lipid synthesis genes in B cells isolated from the mediastinal LN of naive mice, CD23 Cre+/- control mice, and CD23 Cre+ IL-4R flox/flox (IL-4R cKO) mice 5 days post infection (dpi) with 200 PFU of Influenza virus (PR8). Mann Whitney test utilized for statistics
g. qPCR analysis of lipid efflux genes in mediastinal LN B cells from naive mice, CD23 Cre+/- control mice and CD23 Cre+/- IL-4R Flox/flox (cKO) mice 5 days post infection (dpi) with 200 PFU of Influenza virus A (PR8). Mann Whitney test utilized for statistics
h. qPCR analysis of B cells isolated from the spleen and lymph nodes of C57BL/6J mice then stimulated with B cell activating factor (BAFF) [10ng/mL], α-IgM [5μg/mL], α-CD40 [1μg/mL], +/- IL-4 [20ng/mL], +/- IL-21 [20ng/mL] in 10% FBS-supplemented media at listed time points.
i. Heatmaps of bulk RNAseq from WT and STAT6 KO +/- IL-4 [20ng/mL] after 96h activation.

Data are presented as the mean of biological replicates ± s.d. **P*<0.05, ***P*<0.01, ****P*<0.005, *****P*<0.0001 (two-tailed unpaired Student's T-test unless noted otherwise).

Figure 2: Cholesterol promotes cell cycle progression and proliferation in B cells.

a. CellTrace Violet (CTV) traces of B cells isolated from the spleen and lymph nodes of C57BL/6J mice, stimulated with B cell activating factor (BAFF) [10ng/mL], α-IgM [5μg/mL], and α-CD40 [1μg/mL] in 10% FBS-supplemented media, lipid free media + BSA (vehicle), or lipid free media supplemented with water-soluble cholesterol (4ug/mL), BSA-oleic acid (50uM), BSA-palmitic acid (50uM) or with IL-4 [20ng/mL] for 72 or 96h.
b. Summary 96h proliferation data from (A)
c. CTV Summary data of B cells isolated from the spleen and lymph nodes of C57BL/6J mice, stimulated with B cell activating factor (BAFF) [10ng/mL], α-IgM [5μg/mL], and α-CD40 [1μg/mL] in 10% FBS-supplemented media (black bar), lipid free media (white bar) or lipid free media

supplemented with water-soluble cholesterol (2-6ug/mL), with IL-4 [20ng/mL] or IL-21 [40ng/mL] for 48h.

d. Representative flow plots of cell cycle analysis using Ki-67 and 7-AAD
e. Cell cycle analysis of B cells as in (C)
f. qPCR analysis IL-4 responsive genes in B cells isolated from the spleen and lymph nodes of C57BL/6J mice then stimulated with B cell activating factor (BAFF) [10ng/mL], α-IgM [5μg/mL], and α-CD40 [1μg/mL] for 48h +/- IL-4 [20ng/mL] in lipid free media or ± water-soluble cholesterol (final concentration of 4μg/mL).
g. Total (left) and synthesized (right) cholesterol of B cells isolated from the spleen and lymph nodes of C57BL/6J mice–as measured by Isotopic Spectral Analysis (ISA)–following 72h stimulation with B cell activating factor (BAFF) [10ng/mL], α-IgM [5μg/mL], α-CD40 [1μg/mL], +/- IL-4 [20ng/mL] in 10% FBS.
h. Summary proliferation (CTV) data of B cells isolated from the spleen and lymph nodes of C57BL/6J mice then stimulated for 72h with B cell activating factor (BAFF) [10ng/mL], α-IgM [5μg/mL], α-CD40 [1μg/mL], +/- IL-4 [20ng/mL] in lipid free media. Atorvastatin (ATV) administered at a final concentration of 100pM. Water-soluble cholesterol (Chol) administered at a final concentration of 8μg/mL.
i. Cell cycle analysis of B cells isolated from the spleen and lymph nodes of C57BL/6J mice then stimulated for 72h with B cell activating factor (BAFF) [10ng/mL], α-IgM [5μg/mL], α-CD40 [1μg/mL], +/- IL-4 [20ng/mL] in lipid free media. Atorvastatin (ATV) administered at a final concentration of 100pM. Water-soluble cholesterol (Chol) administered at a final concentration of 8μg/mL.

Data are presented as the mean of biological replicates ± s.d. **P*<0.05, ***P*<0.01, ****P*<0.005, *****P*<0.0001 (two-tailed unpaired Welch's T-test). Data are representative of at least two independent experiments.

Figure 3: IL-4 licenses B cell proliferation and cell cycle progression through *de novo* cholesterol synthesis.

a. qPCR gene expression analysis of *Srebf2*$^{flox/flox}$ control (Con) or CD23 Cre+ *Srebf2*$^{flox/flox}$ conditional KO (BP2 cKO) naive B cells stimulated for 48h with B cell activating factor (BAFF) [10ng/mL], α-IgM [5μg/mL], α-CD40 [1μg/mL], +/- IL-4 [20ng/mL] in lipid free media.
b. Summary CTV proliferation data of *Srebf2*$^{flox/flox}$ control (Con) or CD23 Cre+ *Srebf2*$^{flox/flox}$ conditional KO (BP2 cKO) naive B cells stimulated for 48h with B cell activating factor (BAFF) [10ng/mL], α-IgM [5μg/mL], α-CD40 [1μg/mL], +/- IL-4 [20ng/mL], in lipid free media. Water-soluble cholesterol (Chol) administered at indicated final concentrations (μg/mL).
c. Cell cycle analysis summary data of as in (B)

d. Western blot analysis of p21 in *Srebf2*$^{flox/flox}$ control (Con) or CD23 Cre+ *Srebf2*$^{flox/flox}$ conditional KO (BP2 cKO) naive B cells stimulated for 48h with B cell activating factor (BAFF) [10ng/mL], α-IgM [5μg/mL], α-CD40 [1μg/mL], +/- IL-4 [20ng/mL], in lipid free media +/- MBCD cholesterol (Chol). β-Actin is loading control.
e. Viability summary data as in (D).
f. Western blot analysis of cleaved caspase 8 (casp8; p18) as in (D). β-Actin is loading control.
g. Viability summary data of *Srebf2*$^{flox/flox}$ control (Con) or CD23 Cre+ *Srebf2*$^{flox/flox}$ conditional KO (BP2 cKO) naive B cells stimulated for 48h with B cell activating factor (BAFF) [10ng/mL], α-IgM [5μg/mL], α-CD40 [1μg/mL], + IL-4 [20ng/mL] in lipid free media +/- pan-caspase inhibitor, Z-VAD-FMK (P-Caspi) or MBCD- cholesterol (Chol)

Data are presented as the mean of biological replicates ± s.d. **P*<0.05, ***P*<0.01, ***P*<0.005, *****P*<0.0001 (two-tailed unpaired Welch's T-test).

Figure 4: SREBP2-deficient B cells exhibit defective humoral responses *in vivo.*

a. Total number of B cells in the serum of naive *Srebf2*$^{flox/flox}$ control (Con) or CD23 Cre+ *Srebf2*$^{flox/flox}$ conditional KO (BP2 cKO) female mice (*n* = 11).
b. Flow cytometry-based quantification of total number (left) and frequency (right) of plasmablasts in the blood of naive *Srebf2*$^{flox/flox}$ control (Con) or CD23 Cre+ *Srebf2*$^{flox/flox}$ conditional KO (BP2 cKO) female mice (*n* = 11).
c. Total (left) and frequency (right) of proliferating plasmablasts (measured by Ki-67 staining) in the blood of naive *Srebf2*$^{flox/flox}$ control (Con) or CD23 Cre+ *Srebf2*$^{flox/flox}$ conditional KO (BP2 cKO) female mice (*n* = 11).
d. Total number of B cells in the mesenteric lymph nodes of naive *Srebf2*$^{flox/flox}$ control (Con) or CD23 Cre+ *Srebf2*$^{flox/flox}$ conditional KO (BP2 cKO) female mice (*n* = 11).
e. Total number of germinal center (GC) B cells in the mesenteric lymph nodes of naive *Srebf2*$^{flox/flox}$ control (Con) or CD23 Cre+ *Srebf2*$^{flox/flox}$ conditional KO (BP2 cKO) female mice (*n* = 10-11).
f. Frequency of germinal center (GC) B cells in the mesenteric lymph nodes of naive *Srebf2*$^{flox/flox}$ control (Con) or CD23 Cre+ *Srebf2*$^{flox/flox}$ conditional KO (BP2 cKO) female mice (*n* = 10-11).
g. Total proliferating germinal center (GC) B cells (measured by Ki-67 staining) in the mesenteric lymph nodes of naive *Srebf2*$^{flox/flox}$ control (Con) or CD23 Cre+ *Srebf2*$^{flox/flox}$ conditional KO (BP2 cKO) female mice (*n* = 10-11).
h. Total antibody secreting cells (ASCs) in the bone marrow of naive *Srebf2*$^{flox/flox}$ control (Con) or CD23 Cre+ *Srebf2*$^{flox/flox}$ conditional KO (BP2 cKO) male mice (*n*=5-7).
i. Total number (left) and frequency (right) of mature plasma cells (PCs) in the bone marrow of naive *Srebf2*$^{flox/flox}$ control (Con) or CD23 Cre+ *Srebf2*$^{flox/flox}$ conditional KO (BP2 cKO) male mice (*n*=5-7).

j. Total number of B cells in the blood (left) and mediastinal lymph node (right) of *Srebf2*$^{flox/flox}$ control (Con) or CD23 Cre+ *Srebf2*$^{flox/flox}$ conditional KO (BP2 cKO) female mice (*n* =7-8) 6 days post infection (dpi) with 200 PFU of Influenza virus A/Puerto Rico/8/1934 (PR8) H1N1 strain expressing the LCMV gp33-41 epitope (PR8-33).

k. Total number plasmablasts in the blood of *Srebf2*$^{flox/flox}$ control (Con) or CD23 Cre+ *Srebf2*$^{flox/flox}$ conditional KO (BP2 cKO) female mice (*n* = 7-8) 6 days post infection (dpi) with 200 PFU of Influenza virus A/Puerto Rico/8/1934 (PR8) H1N1 strain expressing the LCMV gp33-41 epitope (PR8-33).

l. Total number (left) and frequency (right) of plasmablasts in the mediastinal lymph node of *Srebf2*$^{flox/flox}$ control (Con) or CD23 Cre+ *Srebf2*$^{flox/flox}$ conditional KO (BP2 cKO) female mice (*n* =7-8) 6 days post infection (dpi) as in (I)

m. Total Plasmablasts, GC B cells, and Memory B cells from the mediastinal lymph node 10 days post infection with PR8 influenza as in (J).

Data are presented as the mean of biological replicates ± s.d. **P*<0.05, ***P*<0.01, ****P*<0.005 (two-tailed unpaired Student's T-test).

Figure 5: *De novo* cholesterol synthesis supports IL-4 gene expression, endoplasmic reticulum remodeling, and cell viability.

a. Total (left) and frequency (right) of XBP1s+ plasmablasts in the blood of naive *Srebf2*$^{flox/flox}$ control (Con) or CD23 Cre+ *Srebf2*$^{flox/flox}$ conditional KO (BP2 cKO) female mice (*n* = 10-11).

b. qPCR analysis of XBP1s in *Srebf2*$^{flox/flox}$ control (Con) or CD23 Cre+ *Srebf2*$^{flox/flox}$ conditional KO (BP2 cKO) naive B cells stimulated for 48h with B cell activating factor (BAFF) [10ng/mL], α-IgM [5μg/mL], α-CD40 [1μg/mL], +/- IL-4 [20ng/mL] in lipid free media. Water-soluble cholesterol (Chol) administered at a final concentration of 8μg/mL.

c. Endoplasmic reticulum (ER) mass measured by ER-TrackerTM Green in *Srebf2*$^{flox/flox}$ control (Con) or CD23 Cre+ *Srebf2*$^{flox/flox}$ conditional KO (BP2 cKO) naive B cells stimulated for 48h with B cell activating factor (BAFF) [10ng/mL], α-IgM [5μg/mL], α-CD40 [1μg/mL], +/- IL-4 [20ng/mL] in lipid free media.

d. Endoplasmic reticulum (ER) mass measured by ER-TrackerTM Green in *Srebf2*$^{flox/flox}$ control (Con) or CD23 Cre+ *Srebf2*$^{flox/flox}$ conditional KO (BP2 cKO) naive B cells stimulated for 72h with B cell activating factor (BAFF) [10ng/mL], α-IgM [5μg/mL], α-CD40 [1μg/mL], +/- IL-4 [20ng/mL] in lipid free media. Water-soluble cholesterol (Chol) administered at indicated final concentrations (μg/mL).

e. qPCR gene expression analysis of IL-4/STAT6 dependent genes from *Srebf2*$^{flox/flox}$ control (Con) or CD23 Cre+ *Srebf2*$^{flox/flox}$ conditional KO (BP2 cKO) naive B cells stimulated for 48h with B cell

activating factor (BAFF) [10ng/mL], α-IgM [5μg/mL], α-CD40 [1μg/mL], +/- IL-4 [20ng/mL] in lipid free media. Water-soluble cholesterol (Chol) administered at a final concentration of 8μg/mL.

f. Western blot analysis of phosphorylated (p-) and total STAT6 from whole cell lysates from *Srebf2*$^{flox/flox}$ control (Con) or CD23 Cre+ *Srebf2*$^{flox/flox}$ conditional KO (BP2 cKO) naive B cells stimulated for 48h with B cell activating factor (BAFF) [10ng/mL], α-IgM [5μg/mL], α-CD40 [1μg/mL], IL-4 [20ng/mL] in lipid free media. Water-soluble cholesterol (Chol) administered at a final concentration of 8μg/mL.

g. Summary schematic of how IL-4 signaling licenses B cell activation or drives caspase-mediated apoptosis

Data are presented as the mean of biological replicates ± s.d. **P*<0.05, ***P*<0.01, ****P*<0.005, (two-tailed unpaired Student's T-test).

Extended Figure S1:

a. Schematic of SREBP regulation
b. qPCR gene expression analysis of cholesterol synthesis genes in B cells isolated from the mediastinal lymph node with PR8 influenza A virus at listed time points. Shaded section indicates the peak of IL-4 production by NK T cells.
c. UMAP visualization of WT murine B cells 4 days post infection (dpi) with PR8 influenza A virus colored by relative gene expression values
d. Distribution of mutual information (DREMI) scores between *Il4i1* and all expressed genes.
e. Visualization (DREVI) of relationships between of *Il4i1* versus quiescence/activation and lipid metabolism associated genes.
f. qPCR gene expression analysis of *Prdm1* and *IL4i1* genes in mediastinal LN B cells from naive WT mice, CD23 Cre+/- control mice and CD23 Cre+/- IL-4R$^{flox/flox}$ (cKO) mice 5 dpi with PR8 influenza A virus
g. qPCR gene expression analysis of *Fasn* in mediastinal LN B cells from naive WT mice, CD23 Cre+/- control mice and CD23 Cre+/- IL-4R$^{flox/flox}$ (cKO) mice 5 dpi with PR8 influenza A virus
h. qPCR gene expression analysis of cholesterol synthesis genes time course in naive B cells, or B cells stimulated with B cell activating factor (BAFF) [10ng/mL], α-IgM [5μg/mL], α-CD40 [1μg/mL], +/- IL-4 [20ng/mL], +/- IL-21 [20ng/mL] in 10% FBS-supplemented media.
i. qPCR gene expression analysis of *Il4r* and *Prdm1* time course in naive B cells, or B cells stimulated as in (h) in 10% FBS-supplemented media.
j. qPCR gene expression analysis of *Sdc1*(CD138) time course in naive B cells, or B cells stimulated as in (h) in 10% FBS-supplemented media.
k. qPCR gene expression analysis of cholesterol efflux genes time course in naive B cells, or B cells stimulated as in (h) in 10% FBS-supplemented media.

Data are presented as the mean of biological replicates ± s.d. **P*<0.05, ***P*<0.01, ****P*<0.005, *****P*<0.0001 (two-tailed unpaired Student's T-test unless noted otherwise.)

Extended Figure S2:

a. Proliferation summary data of naive B cells stimulated in 10% fetal bovine serum (FBS)-supplemented media or lipid free media with B cell activating factor (BAFF) [10ng/mL], α-IgM [5μg/mL], α-CD40 [1μg/mL], +/- IL-4 [20ng/mL], as measured by CellTrace Violet (CTV) staining.
b. Representative schematic of isotope tracer analysis of flux into *de novo* cholesterol synthesis pathway

Data are presented as the mean of biological replicates ± s.d. *P<0.05, **P<0.01, ***P<0.005, ****P<0.0001 (two-tailed unpaired Student's T-test unless noted otherwise.)

Extended Figure S3:

a. Proliferation summary data of *Srebf2*$^{flox/flox}$ control (Con) or CD23 Cre+ *Srebf2*$^{flox/flox}$ conditional KO (BP2 cKO) naive B cells stimulated for 48h with B cell activating factor (BAFF) [10ng/mL], α-IgM [5μg/mL], α-CD40 [1μg/mL] in lipid free media. Water-soluble cholesterol (Chol) administered at a final concentration of 8μg/mL.
b. Cell cycle analysis as in (A)
c. Proliferation summary data of *Srebf2*$^{flox/flox}$ control (Con) or CD23 Cre+ *Srebf2*$^{flox/flox}$ conditional KO (BP2 cKO) naive B cells stimulated for 48h with B cell activating factor (BAFF) [10ng/mL], α-IgM [5μg/mL], α-CD40 [1μg/mL], +/- IL-4 [20ng/mL], +/- Mevalonate in lipid free media.
d. Membrane permeability analysis as measured by Sytox Green uptake in *Srebf2*$^{flox/flox}$ control (Con) or CD23 Cre+ *Srebf2*$^{flox/flox}$ conditional KO (BP2 cKO) naive B cells stimulated for 48h with B cell activating factor (BAFF) [10ng/mL], α-IgM [5μg/mL], α-CD40 [1μg/mL] in lipid free media. Water-soluble cholesterol (Chol) administered at a final concentration of 12μg/mL.
e. qPCR gene expression analysis of early BCR responsive genes in *Srebf2*$^{flox/flox}$ control (Con) or CD23 Cre+ *Srebf2*$^{flox/flox}$ conditional KO (BP2 cKO) naive B cells or activated with BAFF[10ng/mL], α-IgM [5μg/mL], α-CD40 [1μg/mL] +/- IL-4 [20ng/mL] for 48h in lipid free media. Water-soluble cholesterol (Chol) administered at a final concentration of 8μg/mL.

   Data are presented as the mean of biological replicates ± s.d. *P<0.05, **P<0.01, ***P<0.005, ****P<0.0001 (two-tailed unpaired Student's T-test unless noted otherwise.)

Extended Figure S4: Normal B cell development in the absence of SREBP2

a. Representative flow cytometry gating by Hardy fraction to define developmental subsets in the bone marrow from *Srebf2*$^{flox/flox}$ control (Con) or CD23 Cre+ *Srebf2*$^{flox/flox}$ conditional KO (BP2 cKO) mice (n=6).
b. Quantification of bone marrow B-cell subsets, showing the frequency (top) and cell number (bottom) of each developmental stage. B220^{+} splenocytes were gated to identify transitional B-cell subsets (T1, T2, and T3) using CD21/CD35 and CD23 expression, and mature B-cell subsets, including marginal zone B cells (MZB) and follicular B cells (FoB).
c. Representative flow cytometry gating strategy of splenic B-cell populations from *Srebf2*$^{flox/flox}$ control (Con) or CD23 Cre+ *Srebf2*$^{flox/flox}$ conditional KO (BP2 cKO) mice.
d. Frequency (top) and total cell number (bottom) of B220^{+} splenocytes from *Srebf2*$^{flox/flox}$ control (Con) or CD23 Cre+ *Srebf2*$^{flox/flox}$ conditional KO (BP2 cKO) mice.

e. Frequencies (left) and total cell numbers (right) of splenic B-cell populations are shown. Data are means ± SEM. Unpaired t tests were used.
f. Representative flow plots of circulating B cells and plasmablasts.

Extended Figure S5:

a. Representative flow plots of GC B cells.
b. Representative flow plots of total B cells, plasmablasts, GC B cells and memory B cells after 6-10 days post infection with PR8 influenza.
c. Representative flow plots of total antibody secreting cells and mature plasma cells in the bone marrow.

Extended Figure S6:

a. Endoplasmic reticulum (ER) mass measured by ER-TrackerTM Green in WT naive B cells stimulated with BAFF [10ng/mL], α-IgM [5μg/mL], α-CD40 [1μg/mL] for 48h +/- IL-4 [20ng/mL] in lipid free media, Atorvastatin (ATV) administered at a final concentration of 100pM. Water-soluble cholesterol (Chol) administered at a final concentration of 8μg/mL.
b. XBP1 transcript levels from bulk RNAseq from WT and STAT6 KO B cells +/- IL-4 [20ng/mL] after 96h activation.
c. IL-4 responsive gene transcript levels from bulk RNAseq from WT and STAT6 KO B cells +/- IL-4 [20ng/mL] after 96h activation.
d. qPCR gene expression analysis of IL-4 responsive genes in *Srebf2*$^{flox/flox}$ control (Con) or CD23 Cre+ *Srebf2*$^{flox/flox}$ conditional KO (BP2 cKO) naive B cells stimulated with BAFF [10ng/mL], α-IgM [5μg/mL], α-CD40 [1μg/mL] for 48h +/- IL-4 [20ng/mL] in lipid free media. Water-soluble cholesterol (Chol) administered at a final concentration of 8μg/mL.

   Data are presented as the mean of biological replicates ± s.d. **P*<0.05, ***P*<0.01, ****P*<0.005, *****P*<0.0001 (two-tailed unpaired Student's T-test unless noted otherwise.)

Figure 1:

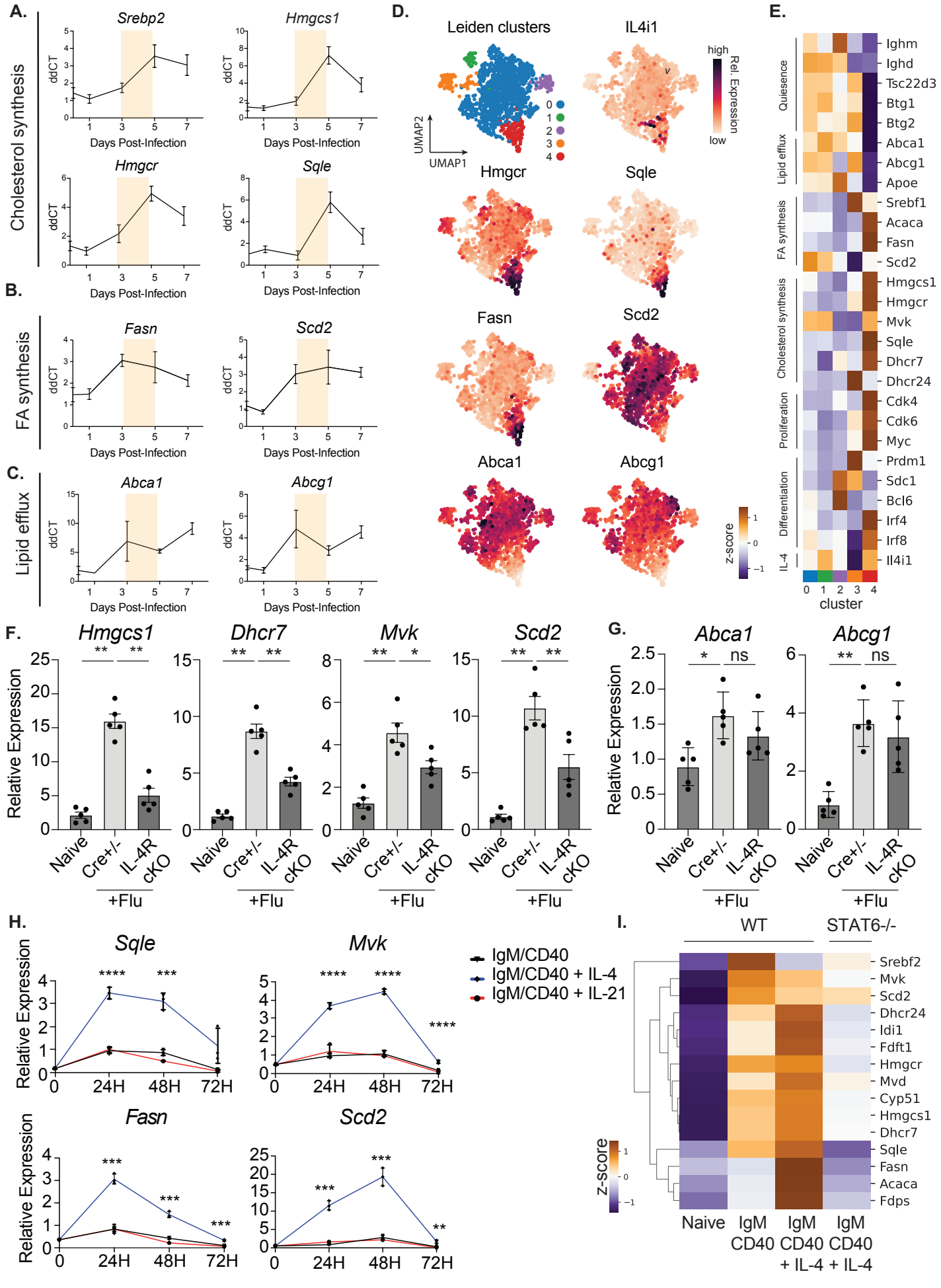

A.
Cholesterol synthesis
Srebp2
Hmgcs1
Hmgcr
Sqle
ddCT
Days Post-Infection
B.
FA synthesis
Fasn
Scd2
C.
Lipid efflux
Abca1
Abcg1
D.
Leiden clusters
IL4i1
high
low
Rel. Expression
UMAP2
UMAP1
Hmgcr
Sqle
Fasn
Scd2
Abca1
Abcg1
z-score
E.
Quiescence
Lipid efflux
FA synthesis
Cholesterol synthesis
Proliferation
Differentiation
IL-4
Ighm
Ighd
Tsc22d3
Btg1
Btg2
Abca1
Abcg1
Apoe
Srebf1
Acaca
Fasn
Scd2
Hmgcs1
Hmgcr
Mvk
Sqle
Dhcr7
Dhcr24
Cdk4
Cdk6
Myc
Prdm1
Sdc1
Bcl6
Irf4
Irf8
Il4i1
cluster
F.
Hmgcs1
Dhcr7
Mvk
Scd2
Relative Expression
Naive
Cre+/-
IL-4R cKO
+Flu
G.
Abca1
Abcg1
ns
H.
Sqle
Mvk
Fasn
Scd2
Relative Expression
24H
48H
72H
IgM/CD40
IgM/CD40 + IL-4
IgM/CD40 + IL-21
I.
WT
STAT6-/-
Srebf2
Mvk
Scd2
Dhcr24
Idi1
Fdft1
Hmgcr
Mvd
Cyp51
Hmgcs1
Dhcr7
Sqle
Fasn
Acaca
Fdps
z-score
Naive
IgM CD40
IgM CD40 + IL-4
IgM CD40 + IL-4

Figure 2:

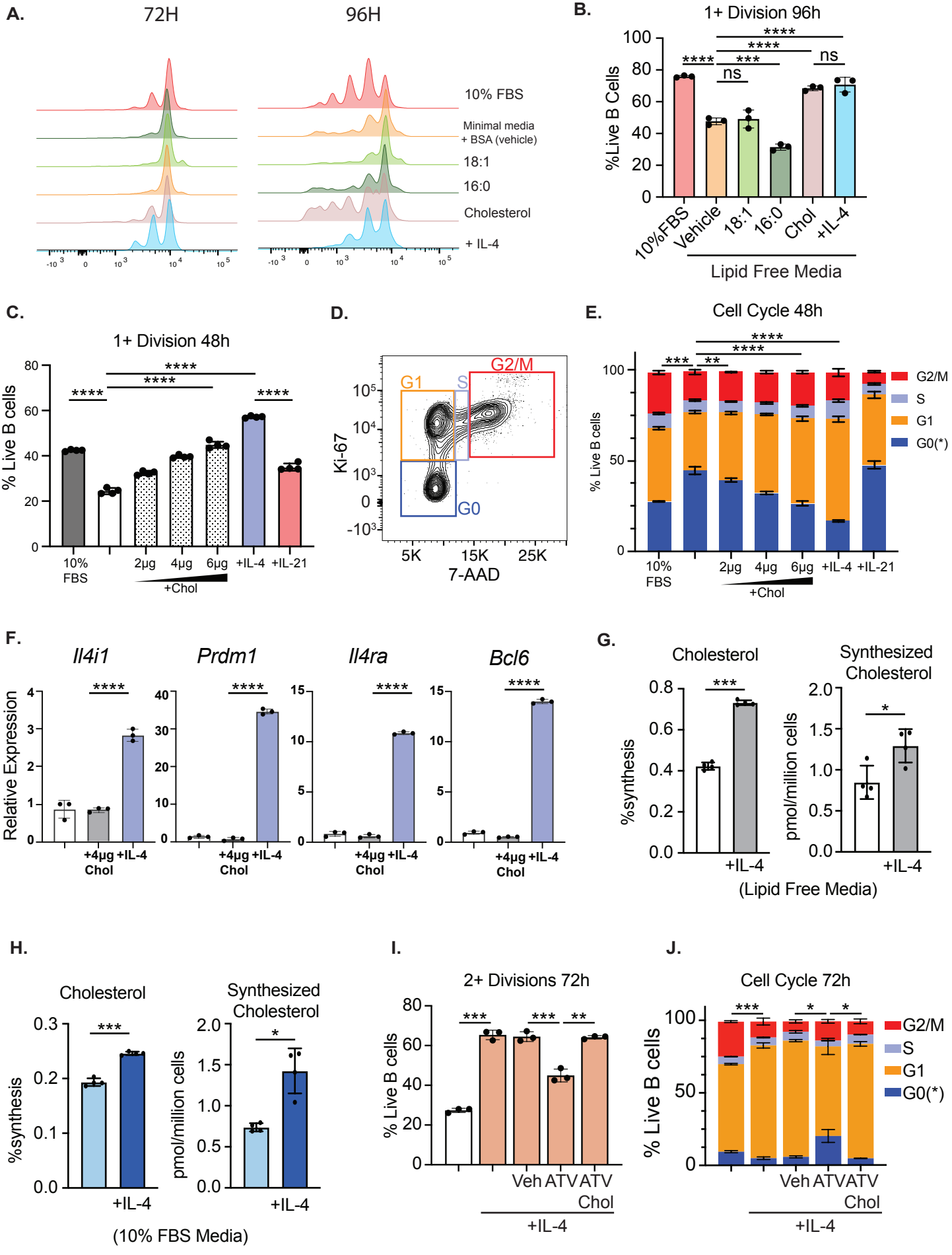

A.
72H
96H
10% FBS
Minimal media
+ BSA (vehicle)
18:1
16:0
Cholesterol
+ IL-4
B.
1+ Division 96h
%Live B Cells
10%FBS
Vehicle
18:1
16:0
Chol
+IL-4
Lipid Free Media
C.
1+ Division 48h
% Live B cells
10%
FBS
2µg
4µg
6µg
+IL-4
+IL-21
+Chol
D.
G1
S
G2/M
G0
Ki-67
7-AAD
E.
Cell Cycle 48h
% Live B cells
G2/M
S
G1
G0(*)
F.
Il4i1
Prdm1
Il4ra
Bcl6
Relative Expression
+4µg Chol
+IL-4
G.
Cholesterol
Synthesized Cholesterol
%synthesis
pmol/million cells
+IL-4
(Lipid Free Media)
H.
Cholesterol
Synthesized Cholesterol
%synthesis
pmol/million cells
+IL-4
(10% FBS Media)
I.
2+ Divisions 72h
% Live B cells
Veh
ATV
ATV Chol
+IL-4
J.
Cell Cycle 72h
% Live B cells
G2/M
S
G1
G0(*)
Veh
ATV
ATV Chol
+IL-4

Figure 3:

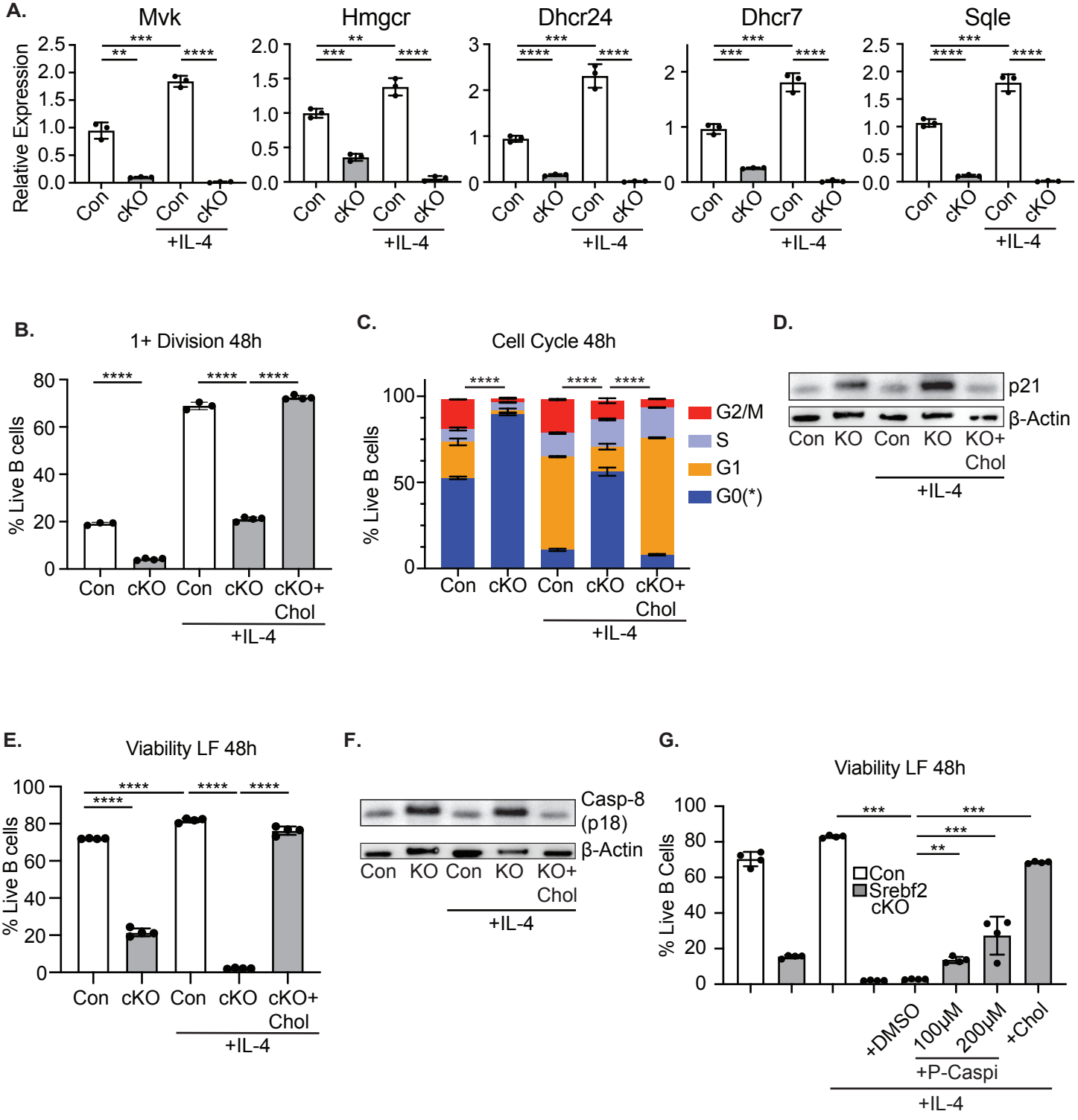

A.
Mvk
Hmgcr
Dhcr24
Dhcr7
Sqle
Relative Expression
Con
cKO
+IL-4
B.
1+ Division 48h
% Live B cells
cKO+ Chol
C.
Cell Cycle 48h
G2/M
S
G1
G0(*)
D.
p21
β-Actin
KO
KO+ Chol
E.
Viability LF 48h
F.
Casp-8 (p18)
G.
Viability LF 48h
% Live B Cells
Con
Srebf2 cKO
+DMSO
100μM
200μM
+Chol
+P-Caspi

Figure 4:

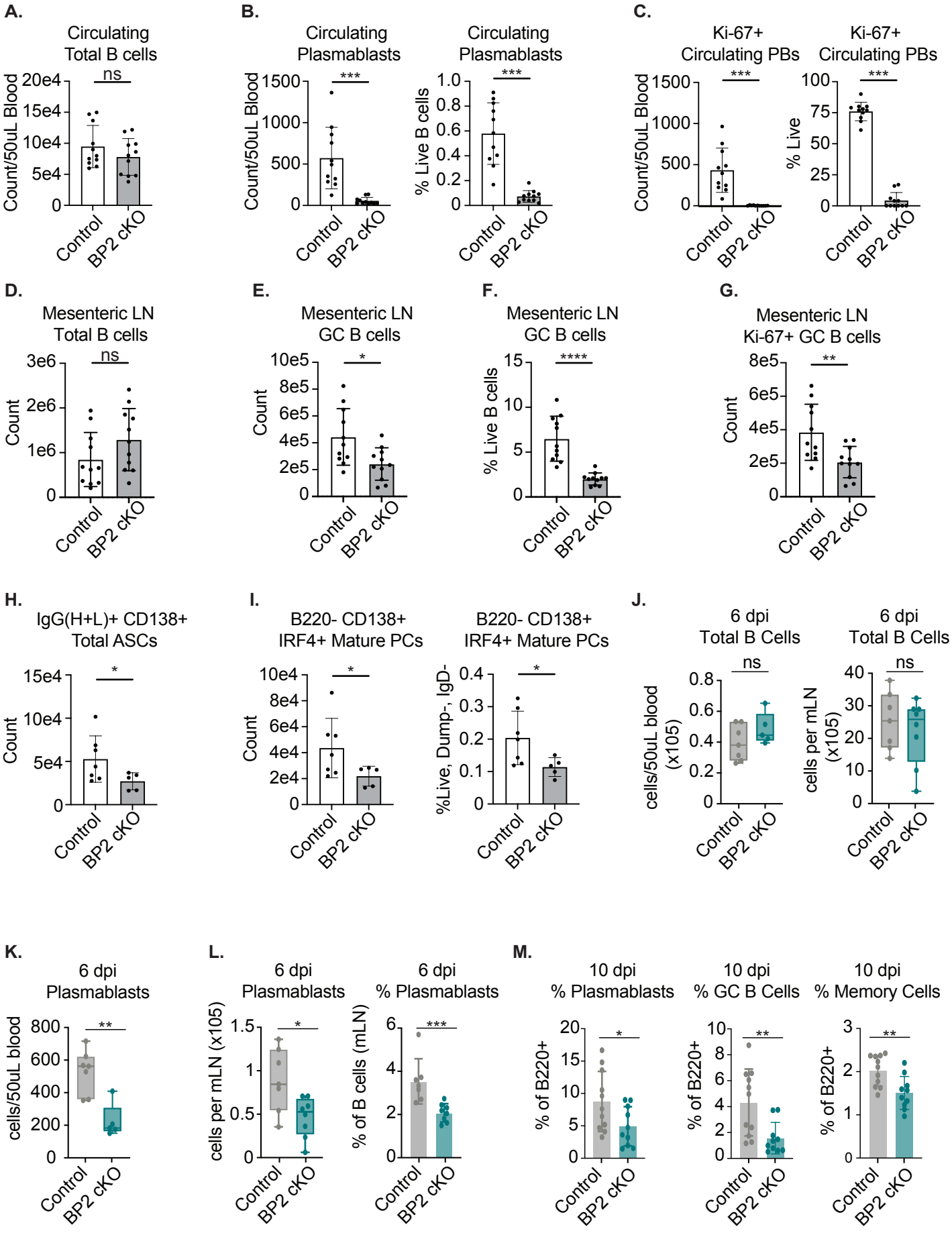
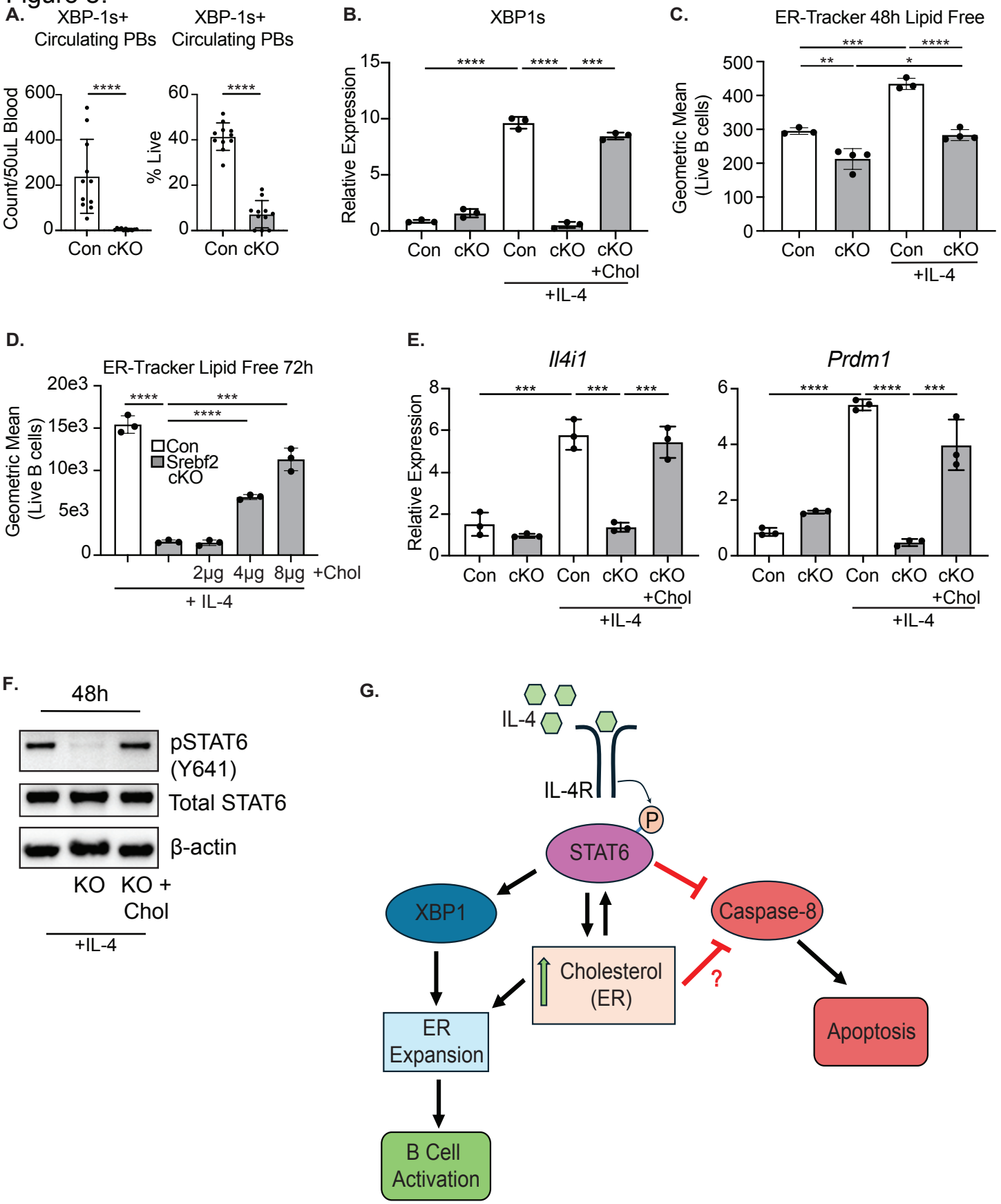
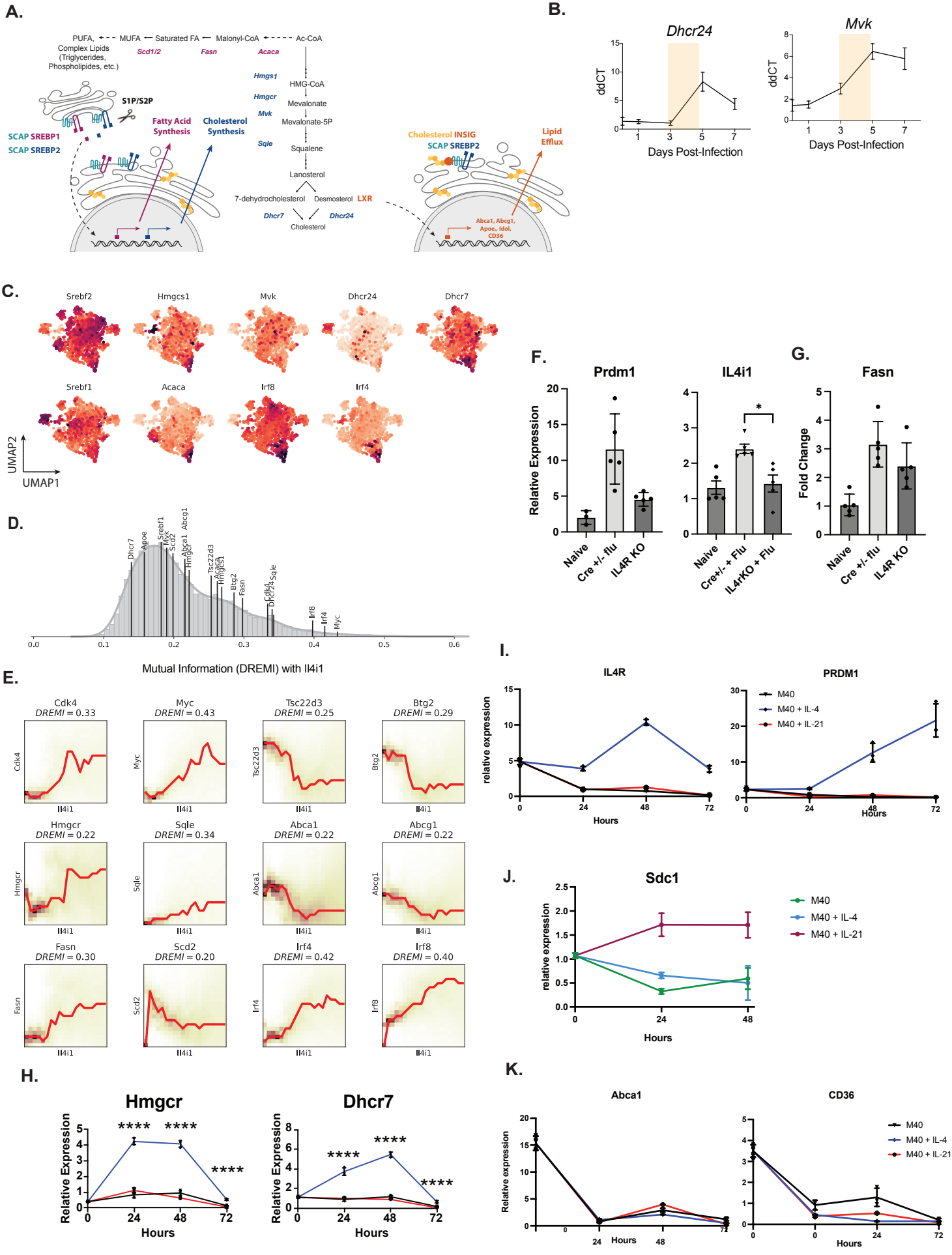

A.
Circulating
Total B cells
Count/50uL Blood
20e4
15e4
10e4
5e4
0
ns
Control
BP2 cKO
B.
Circulating
Plasmablasts
Count/50uL Blood
1500
1000
500
0
***
Circulating
Plasmablasts
% Live B cells
1.0
0.8
0.6
0.4
0.2
0
***
C.
Ki-67+
Circulating PBs
Count/50uL Blood
1500
1000
500
0
***
Ki-67+
Circulating PBs
% Live
100
75
50
25
0
***
D.
Mesenteric LN
Total B cells
Count
3e6
2e6
1e6
0
ns
E.
Mesenteric LN
GC B cells
Count
10e5
8e5
6e5
4e5
2e5
0
*
F.
Mesenteric LN
GC B cells
% Live B cells
15
10
5
0
****
G.
Mesenteric LN
Ki-67+ GC B cells
Count
8e5
6e5
4e5
2e5
0
**
H.
IgG(H+L)+ CD138+
Total ASCs
Count
15e4
10e4
5e4
0
*
I.
B220- CD138+
IRF4+ Mature PCs
Count
10e4
8e4
6e4
4e4
2e4
0
*
B220- CD138+
IRF4+ Mature PCs
%Live, Dump-, IgD-
0.4
0.3
0.2
0.1
0
*
J.
6 dpi
Total B Cells
cells/50uL blood
(x105)
0.8
0.6
0.4
0.2
0
ns
6 dpi
Total B Cells
cells per mLN
(x105)
40
30
20
10
0
ns
K.
6 dpi
Plasmablasts
cells/50uL blood
800
600
400
200
0
**
L.
6 dpi
Plasmablasts
cells per mLN (x105)
1.5
1
0.5
0
*
6 dpi
% Plasmablasts
% of B cells (mLN)
6
4
2
0
***
M.
10 dpi
% Plasmablasts
% of B220+
20
15
10
5
0
*
10 dpi
% GC B Cells
% of B220+
10
8
6
4
2
0
**
10 dpi
% Memory Cells
% of B220+
3
2
1
0
**
Control
BP2 cKO

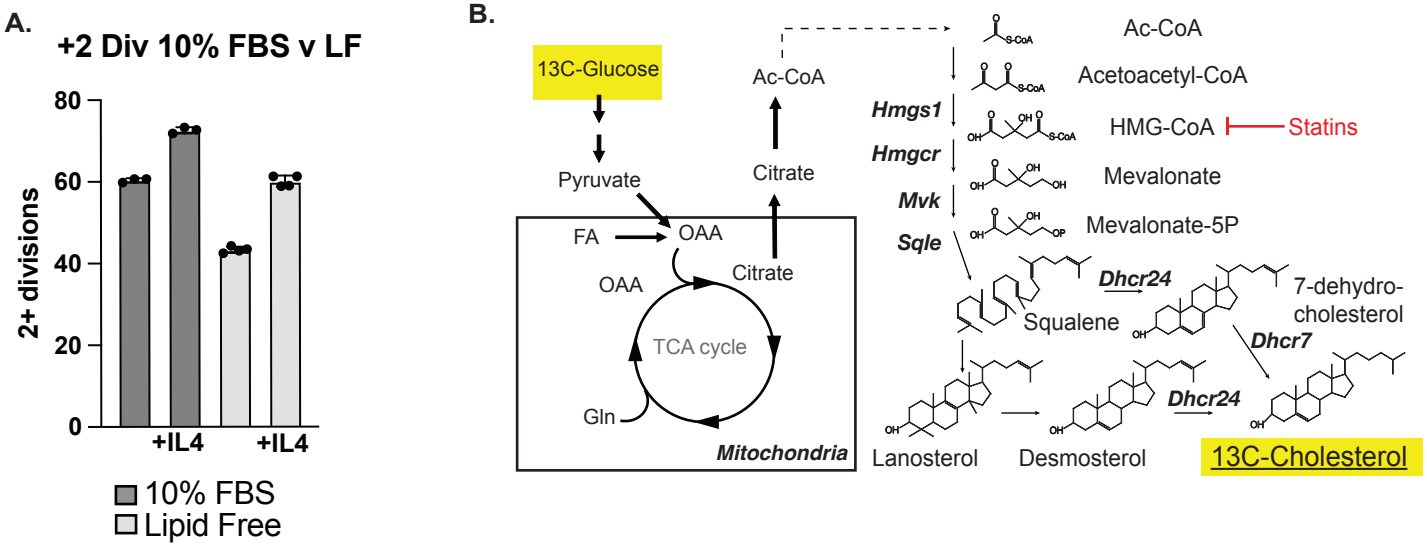
Figure 5:


A.
XBP-1s+ Circulating PBs
Count/50uL Blood
% Live
Con cKO
B.
XBP1s
Relative Expression
+IL-4
+Chol
C.
ER-Tracker 48h Lipid Free
Geometric Mean (Live B cells)
D.
ER-Tracker Lipid Free 72h
Srebf2 cKO
2µg 4µg 8µg +Chol
+ IL-4
E.
Il4i1
Prdm1
F.
48h
pSTAT6 (Y641)
Total STAT6
β-actin
KO KO + Chol
G.
IL-4
IL-4R
P
STAT6
XBP1
Caspase-8
Cholesterol (ER)
ER Expansion
Apoptosis
B Cell Activation

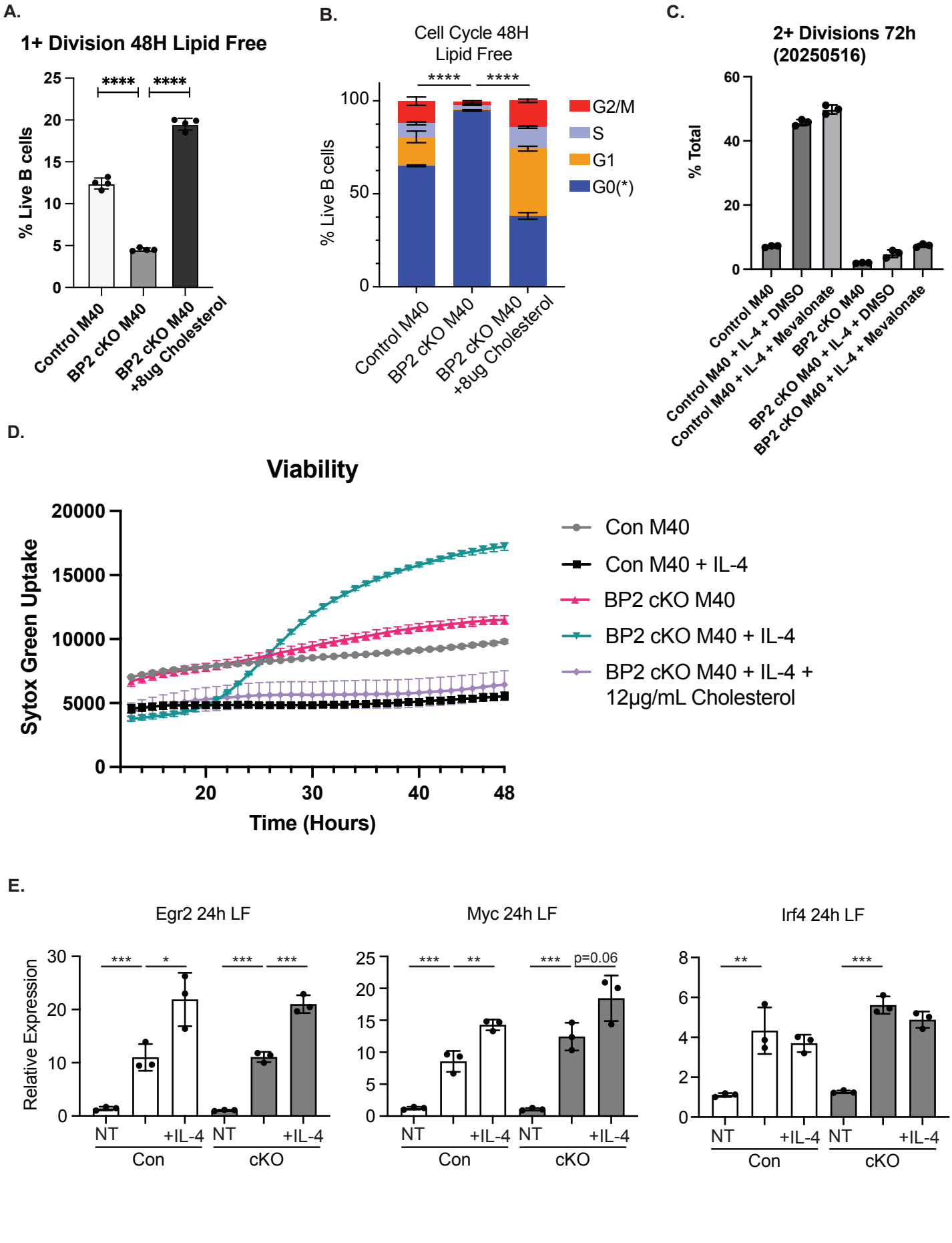
Extended Figure S1:



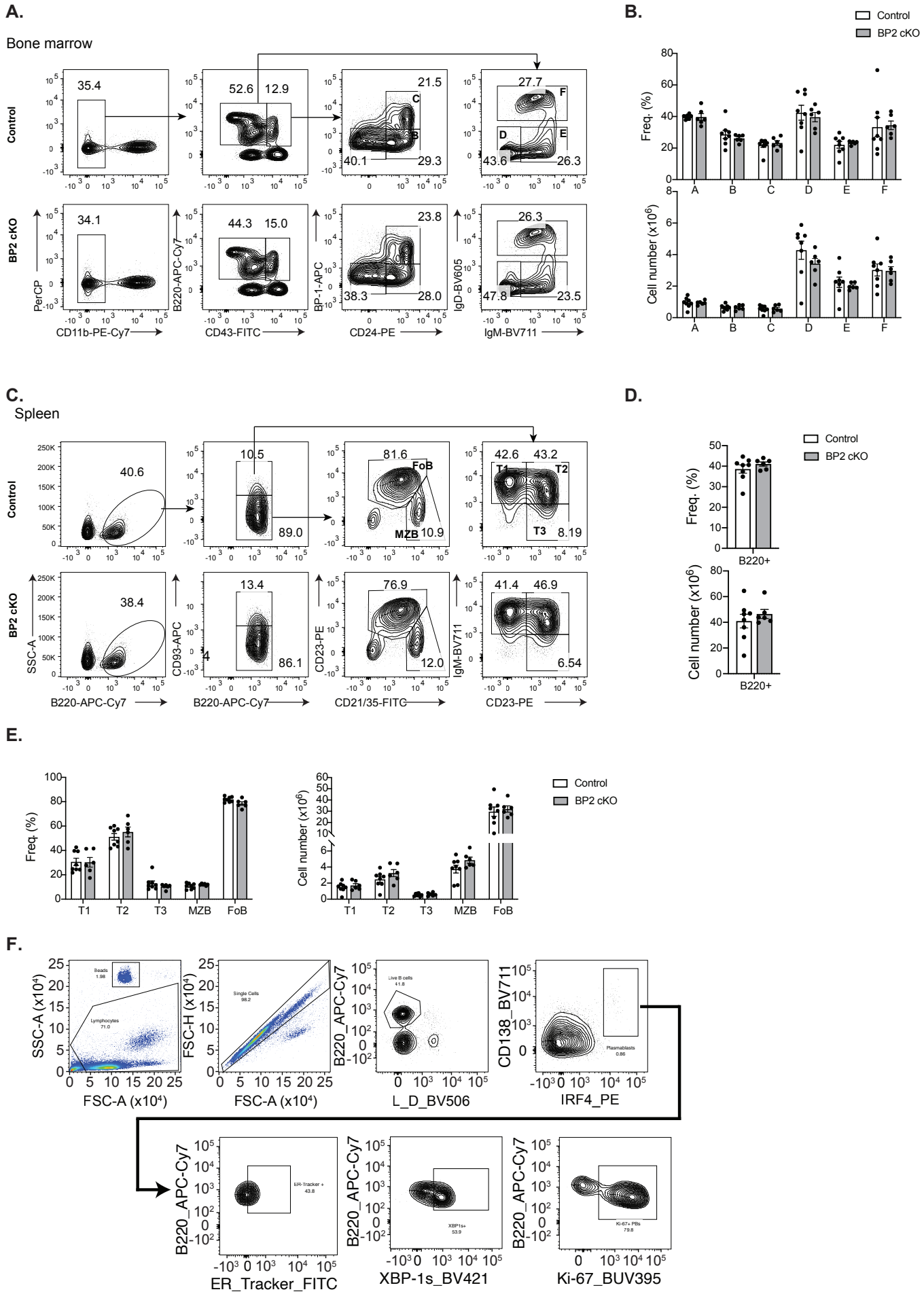
Extended figure S2



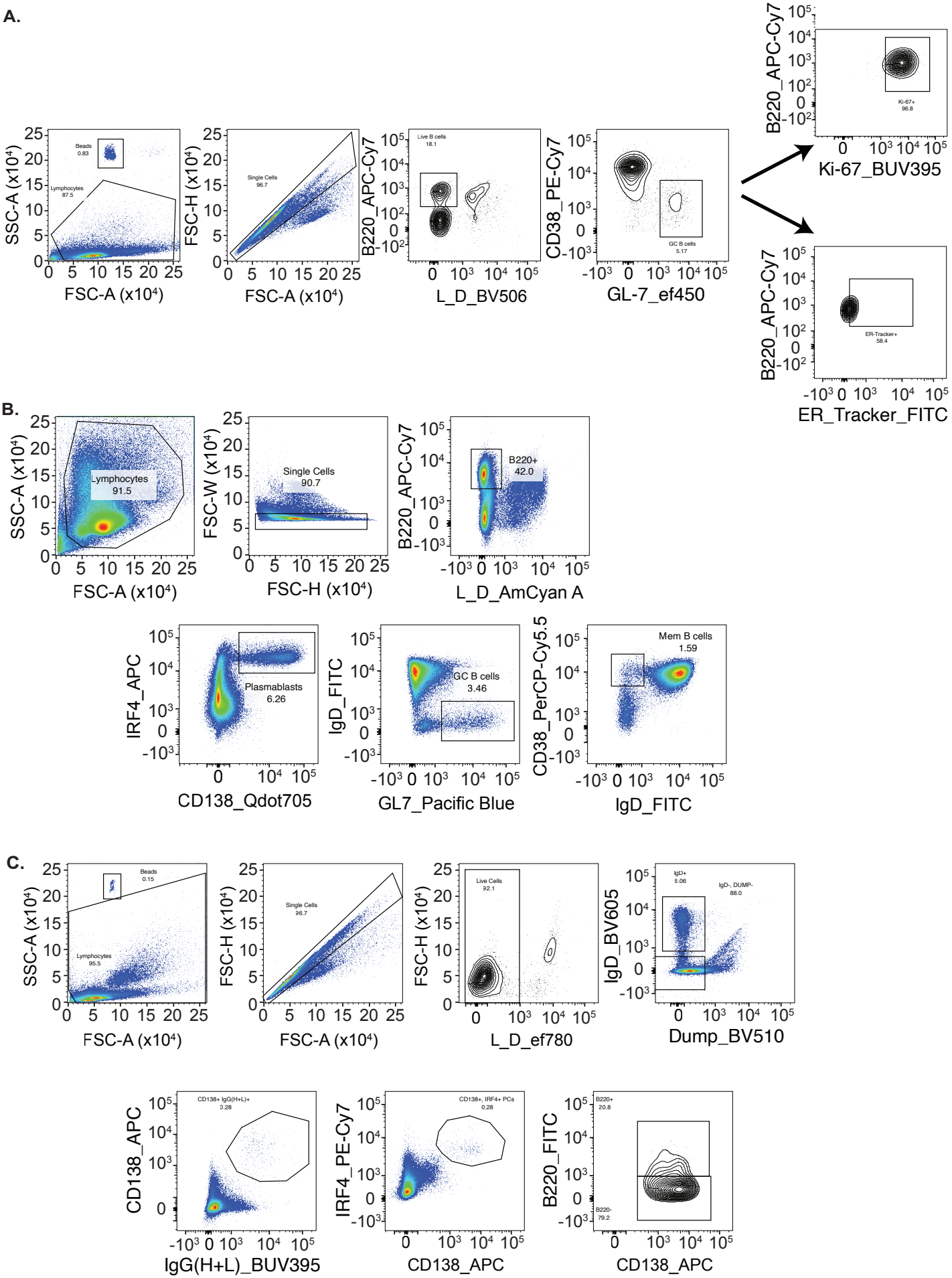
Extended figure S3



Extended figure S4



Extended figure S5:



Extended figure S6:

